INTERNATIONAL JOURNAL FOR NUMERICAL METHODS IN FLUIDS
Int. J. Numer. Meth. Fluids 2007; **53**:599–627
Published online 20 September 2006 in Wiley InterScience (www.interscience.wiley.com). DOI: 10.1002/fld.1298

Solving viscoelastic free surface flows of a second-order fluid using a marker-and-cell approach

M. F. Tomé[1,‡], J. L. Doricio[1,§], A. Castelo[1,¶], J. A. Cuminato[1,‖] and S. McKee[2,*,†]

[1]*Instituto de Ciências Matemáticas e de Computação, ICMC, USP, Av. do Trabalhador São Carlense, 400-Centro, 13560-970, Cx. Postal: 668, São Carlos, SP, Brazil*
[2]*Department of Mathematics, University of Strathclyde, Glasgow, U.K.*

SUMMARY

This work is concerned with the numerical simulation of two-dimensional viscoelastic free surface flows of a second-order fluid. The governing equations are solved by a finite difference technique based on the marker-and-cell philosophy. A staggered grid is employed and marker particles are used to represent the fluid free surface. Full details for the approximation of the free surface stress conditions are given. The resultant code is validated and convergence is demonstrated. Numerical simulations of the extrudate swell and flow through a planar 4:1 contraction for various values of the Deborah number are presented. Copyright © 2006 John Wiley & Sons, Ltd.

Received 30 June 2005; Revised 2 April 2006; Accepted 27 April 2006

KEY WORDS: free surface flow; marker-and-cell; second-order fluid; finite difference

1. INTRODUCTION

Industrial polymer processing frequently involves free surface flows of a complex fluid. Examples of these are extrusion, fibre-spinning, container filling and wire coating. These problems have

*Correspondence to: S. McKee, Department of Mathematics, University of Strathclyde, Glasgow, U.K.
†E-mail: smck@maths.strath.ac.uk
‡E-mail: murilo@icmc.usp.br
§E-mail: josedoricio@yahoo.com.br
¶E-mail: castelo@icmc.usp.br
‖E-mail: jacumina@icmc.usp.br

Contract/grant sponsor: FAPESP (Fundação de Amparo a pesquisa do Estado de São Paulo); contract/grant number: 00/03385-0
Contract/grant sponsor: CAPES (Coordenação de Aperfeiçoamento de Pessoal de Nível Superior); contract/grant number: 136/05-CAPES/GRICES
Contract/grant sponsor: CNPq (Conselho Nacional de Desenvolvimento Científico e Tecnológico); contract/grant numbers: 474040/2003-8, 523141/94

Copyright © 2006 John Wiley & Sons, Ltd.

contributed to the motivation of the development of numerical methods so that these processes may be studied through simulation. The Maxwell, Oldroyd-B and PTT models have been considered by many researchers and a variety of techniques for simulating viscoelastic flows governed by these models have been presented, e.g. References [1–7], to cite a few. The problems investigated have been the contraction 4:1 problem in both two dimensions (e.g. References [5, 7, 8]), and in three dimensions (e.g. References [6, 9]); extrudate swell problems have been considered by, among others, Brasseur *et al.* [1], Ryan and Dutta [10], Crochet and Keunings [11] and Tomé *et al.* [12].

On the other hand, less attention has been paid to viscoelastic flows governed by the Criminale–Ericksen–Filbey (CEF) constitutive relationship, which is sometimes simply known as the second-order fluid. Gast and Ellington [13] employed the Fidap code [14] to compute extrudate swells for the CEF equation in the case of a fluid where the viscoelasticity was minimal.

The purpose of this work is to present a numerical method for solving the two-dimensional second-order fluid flow model, which is capable of resolving free surface flows where the viscoelasticity is not necessarily small. We formulate a MAC (marker-and-cell)-type [15] numerical algorithm for solving the governing equations and develop a finite difference method for solving the basic equations. The method described herein is validated by using exact solutions for two-dimensional channel flow; numerical results of the time-dependent extrudate swell and 4:1 contraction flows are also presented to illustrate the capability of the method.

2. BASIC EQUATIONS

The equations governing the flow of a second-order fluid are (see Reference [16]) the equation of motion

$$\rho\left(\frac{\partial \mathbf{u}}{\partial t}+\nabla\cdot\mathbf{uu}\right)=-\nabla p+\nabla\cdot\boldsymbol{\tau}+\rho\mathbf{g} \tag{1}$$

and the mass conservation equation (assuming incompressibility)

$$\nabla\cdot\mathbf{u}=0 \tag{2}$$

where $\boldsymbol{\tau}$ is the extra-stress tensor which obeys the constitutive equation

$$\boldsymbol{\tau}=\eta_0[\mathbf{D}+\lambda_2\overset{\triangledown}{\mathbf{D}}+\lambda_4(\mathbf{D}\cdot\mathbf{D})] \tag{3}$$

The parameters η_0, λ_2 and λ_4 are material properties and $\mathbf{D}$ is the rate-of-deformation tensor. The tensor $\mathbf{D}$ and the upper convected derivative $\overset{\triangledown}{\mathbf{D}}$ are given by

$$\mathbf{D}=(\nabla\mathbf{u})+(\nabla\mathbf{u})^{\mathrm{T}},\quad \overset{\triangledown}{\mathbf{D}}=\frac{D}{Dt}\mathbf{D}-(\nabla\mathbf{u})^{\mathrm{T}}\mathbf{D}-\mathbf{D}(\nabla\mathbf{u}) \tag{4}$$

respectively. The symbol D/Dt refers to the material derivative and is defined by

$$\frac{D}{Dt}\mathbf{D}=\frac{\partial\mathbf{D}}{\partial t}+\nabla\cdot(\mathbf{uD})$$

Here, as usual, $\mathbf{u}$, $\boldsymbol{\tau}$, p, ρ, denote the fluid velocity, the extra-stress tensor, pressure and density, respectively, while $\mathbf{g}$ denotes the gravitational field.

Copyright © 2006 John Wiley & Sons, Ltd.

DOI: 10.1002/fld

In order to solve Equations (1)–(3) it is necessary to specify initial and boundary conditions for $\mathbf{u}$. On rigid boundaries it is sufficient to have the no-slip condition ($\mathbf{u}=0$) and on inflows the velocity is assumed to be given: $\mathbf{u}=U_{\text{inf}}$. We consider a viscous fluid flowing into a passive atmosphere (which we take to be at zero pressure) so that the normal and tangential components of stress must be continuous across the free surface. In this work, we assume that surface tension effects can be ignored so that, on the free surface, the conditions that must be satisfied are (see Referfence [17])

$$\mathbf{n}\cdot(\boldsymbol{\sigma}\cdot\mathbf{n})=0 \quad \text{and} \quad \mathbf{m}\cdot(\boldsymbol{\sigma}\cdot\mathbf{n})=0 \tag{5}$$

where $\mathbf{n}$ and $\mathbf{m}$ denote unit normal and tangent vectors to the surface and $\boldsymbol{\sigma}=-p\mathbf{I}+\boldsymbol{\tau}$ is the stress tensor.

We shall investigate two-dimensional free surface flows using Cartesian coordinates. In this case, the constitutive equation (3) can be written in the form

$$\boldsymbol{\tau}=\begin{bmatrix}\tau^{xx} & \tau^{xy}\\ \tau^{xy} & \tau^{yy}\end{bmatrix}$$

where

$$\tau^{xx}=\eta_0(D^{xx}+\Phi^{xx}), \quad \tau^{xy}=\eta_0(D^{xy}+\Phi^{xy}), \quad \tau^{yy}=\eta_0(D^{yy}+\Phi^{yy}) \tag{6}$$

and the rheological functions Φ^{xx}, Φ^{xy} and Φ^{yy} can be gathered in the form

$$\Phi^{xx}=\lambda_4\left[4\left(\frac{\partial u}{\partial x}\right)^2+\left(\frac{\partial u}{\partial y}+\frac{\partial v}{\partial x}\right)^2\right]-\lambda_2\left[-\frac{D(D^{xx})}{Dt}+4\left(\frac{\partial u}{\partial x}\right)^2+2\frac{\partial u}{\partial y}\left(\frac{\partial u}{\partial y}+\frac{\partial v}{\partial x}\right)\right] \tag{7}$$

$$\Phi^{xy}=-2\lambda_2\left[-\frac{D(D^{xy})}{Dt}+\frac{\partial u}{\partial x}\frac{\partial v}{\partial x}+\frac{\partial u}{\partial y}\frac{\partial v}{\partial y}\right] \tag{8}$$

$$\Phi^{yy}=\lambda_4\left[4\left(\frac{\partial v}{\partial y}\right)^2+\left(\frac{\partial u}{\partial y}+\frac{\partial v}{\partial x}\right)^2\right]-\lambda_2\left[-\frac{D(D^{yy})}{Dt}+4\left(\frac{\partial v}{\partial y}\right)^2+2\frac{\partial v}{\partial x}\left(\frac{\partial u}{\partial y}+\frac{\partial v}{\partial x}\right)\right] \tag{9}$$

respectively. The components of the rate-of-deformation tensor are defined by Equation (4) and may be written as

$$D^{xx}=2\frac{\partial u}{\partial x}, \quad D^{xy}=\frac{\partial u}{\partial y}+\frac{\partial v}{\partial x}, \quad D^{yy}=2\frac{\partial v}{\partial y} \tag{10}$$

The equation of motion (1) may be written as

$$\frac{\partial u}{\partial t}+\frac{\partial u^2}{\partial x}+\frac{\partial uv}{\partial y}=-\frac{\partial p}{\partial x}+\frac{\eta_0}{\rho}\left[\frac{\partial^2 u}{\partial x^2}+\frac{\partial^2 u}{\partial y^2}+\frac{\partial \Phi^{xx}}{\partial x}+\frac{\partial \Phi^{xy}}{\partial y}\right]+g_x \tag{11}$$

$$\frac{\partial v}{\partial t}+\frac{\partial uv}{\partial x}+\frac{\partial v^2}{\partial y}=-\frac{\partial p}{\partial y}+\frac{\eta_0}{\rho}\left[\frac{\partial^2 v}{\partial x^2}+\frac{\partial^2 v}{\partial y^2}+\frac{\partial \Phi^{xy}}{\partial x}+\frac{\partial \Phi^{yy}}{\partial y}\right]+g_y \tag{12}$$

using (6) and the continuity equation (2).

Copyright © 2006 John Wiley & Sons, Ltd.

DOI: 10.1002/fld

Let L, U denote reference values for length and velocity. To solve Equations (7)–(12) we shall employ the following nondimensionalization:

$$x = L\bar{x}, \quad y = L\bar{y}, \quad u = U\bar{u}, \quad v = U\bar{v}, \quad t = \frac{L}{U}\bar{t}, \quad p = \rho U^2 \bar{p} \tag{13}$$

Introducing (13) into Equations (6)–(12) we obtain the nondimensional equations (the bars have been dropped for clarity)

$$\frac{\partial u}{\partial x} + \frac{\partial v}{\partial y} = 0 \tag{14}$$

$$\frac{\partial u}{\partial t} + \frac{\partial u^2}{\partial x} + \frac{\partial uv}{\partial y} = -\frac{\partial p}{\partial x} + \frac{1}{Re}\left[\frac{\partial^2 u}{\partial x^2} + \frac{\partial^2 u}{\partial y^2} + \frac{\partial \Phi^{xx}}{\partial x} + \frac{\partial \Phi^{xy}}{\partial y}\right] + \frac{1}{Fr^2} g_x \tag{15}$$

$$\frac{\partial v}{\partial t} + \frac{\partial uv}{\partial x} + \frac{\partial v^2}{\partial y} = -\frac{\partial p}{\partial y} + \frac{1}{Re}\left[\frac{\partial^2 v}{\partial x^2} + \frac{\partial^2 v}{\partial y^2} + \frac{\partial \Phi^{xy}}{\partial x} + \frac{\partial \Phi^{yy}}{\partial y}\right] + \frac{1}{Fr^2} g_y \tag{16}$$

$$\tau^{xx} = \frac{1}{Re}(D^{xx} + \Phi^{xx}), \quad \tau^{xy} = \frac{1}{Re}(D^{xy} + \Phi^{xy}), \quad \tau^{yy} = \frac{1}{Re}(D^{yy} + \Phi^{yy}) \tag{17}$$

where D^{xx}, D^{xy} and D^{yy} are given by (10) and the rheological functions can be written as

$$\Phi^{xx} = \kappa\left[4\left(\frac{\partial u}{\partial x}\right)^2 + \left(\frac{\partial u}{\partial y} + \frac{\partial v}{\partial x}\right)^2\right] - De\left[-\frac{D(D^{xx})}{Dt} + 4\left(\frac{\partial u}{\partial x}\right)^2 + 2\frac{\partial u}{\partial y}\left(\frac{\partial u}{\partial y} + \frac{\partial v}{\partial x}\right)\right] \tag{18}$$

$$\Phi^{xy} = -2De\left[-\frac{D(D^{xy})}{Dt} + \frac{\partial u}{\partial x}\frac{\partial v}{\partial x} + \frac{\partial u}{\partial y}\frac{\partial v}{\partial y}\right] \tag{19}$$

$$\Phi^{yy} = \kappa\left[4\left(\frac{\partial v}{\partial y}\right)^2 + \left(\frac{\partial u}{\partial y} + \frac{\partial v}{\partial x}\right)^2\right] - De\left[-\frac{D(D^{yy})}{Dt} + 4\left(\frac{\partial v}{\partial y}\right)^2 + 2\frac{\partial v}{\partial x}\left(\frac{\partial u}{\partial y} + \frac{\partial v}{\partial x}\right)\right] \tag{20}$$

where $Re = \rho U L/\eta_0$, $Fr = U/\sqrt{Lg}$, $De = \lambda_2 U/L$ are the Reynolds number, the Froude number and the Deborah number, respectively. The nondimensional number κ is defined by $\kappa = \lambda_4 U/L$. In steady shear flows, the material parameters λ_2 and λ_4 are related to the coefficients of the first and second normal stress differences

$$\lambda_2 = \frac{1}{2\eta_0}\frac{N_1}{(D^{xy})^2} \tag{21}$$

$$\lambda_4 = \frac{1}{2\eta_0}\frac{N_2}{(D^{yz})^2} \tag{22}$$

where $N_1 = \tau^{xx} - \tau^{yy}$ and $N_2 = \tau^{yy} - \tau^{zz}$ are the first and second normal stress differences, respectively. The material parameter λ_4 is found, experimentally, to be much less than λ_2 (see Reference [16]) and so, henceforth, λ_4 will be neglected.

Copyright © 2006 John Wiley & Sons, Ltd.

DOI: 10.1002/fld

2.1. Computation of the rheological function Φ^{xy} on rigid boundaries and inflows and outflows

When solving (15) and (16) the values of Φ^{xy} are required both on inflows and outflows and also required on the rigid boundaries. These can be obtained from (19) as follows.

- *Rigid boundaries*. If we consider rigid boundaries which are parallel to the x-axis we have

$$\frac{\partial u}{\partial x}=0, \quad \frac{\partial v}{\partial x}=0 \quad \text{and consequently } \frac{\partial v}{\partial y}=0, \text{ from mass conservation}$$

  By introducing these derivatives into (19) it is not difficult to show that $\Phi^{xy}=0$ on the rigid boundaries that are either parallel to the x-axis or to the y-axis.
- *Inflows*. If the velocity at the inflow is prescribed by $u=U_{\text{inf}}$ and $v=V_{\text{inf}}$ then the values of Φ^{xy} on inflows are the same as those for Φ^{xy} on rigid boundaries. However, we shall have inflows defined by $u=u(y)$, $v=0$ if the inflow is vertical, or $u=0$, $v=v(x)$ if the inflow is horizontal; the velocity $u(y)$ (or $v(x)$) is a parabolic function of y (or x). In this case, it can be shown that the value of Φ^{xy} on inflows is zero.
- *Outflows*. At the fluid exit we have the condition $\partial u_T/\partial n=0$ where u_T is the tangential velocity to the outflow and n is the normal direction. Thus, if the outflow is situated parallel to the y-axis we have $\partial v/\partial x=0$; in this case, it can be found that $\Phi^{xy}=0$.

3. NUMERICAL METHOD

To solve Equations (14)–(20) we employ a methodology based on the GENSMAC algorithm (see Reference [18]). We suppose that the velocity field $\mathbf{u}(\mathbf{x}, t_n)$ is known and boundary conditions for velocity and pressure are given. The velocity and pressure fields at time $t=t_n+\delta t$ are calculated as follows.

First, by using $\mathbf{u}(\mathbf{x}, t_n)$ we compute the components of the rate-of-deformation tensor, D^{xx}, D^{xy} and D^{yy} and then calculate the rheological functions Φ^{xx}, Φ^{xy}, Φ^{yy} everywhere on the mesh; the finite difference equations for calculating Φ^{xx}, Φ^{xy}, Φ^{yy} are given in Section 4.1. Now, let $\tilde{p}(\mathbf{x}, t)$ be a pressure field which coincides with the correct pressure condition on the free surface. This pressure field is calculated from Equation (5); details on the calculation of $\tilde{p}(\mathbf{x}, t)$ are given in Section 4.2. Inserting $\tilde{p}(\mathbf{x}, t)$ into (15) and (16) we compute an intermediate velocity field $\tilde{\mathbf{u}}(\mathbf{x}, t)$ from

$$\frac{\partial \tilde{u}}{\partial t}+\frac{\partial u^2}{\partial x}+\frac{\partial uv}{\partial y}=-\frac{\partial \tilde{p}}{\partial x}+\frac{1}{Re}\left[\frac{\partial^2 u}{\partial x^2}+\frac{\partial^2 u}{\partial y^2}+\frac{\partial \Phi^{xx}}{\partial x}+\frac{\partial \Phi^{xy}}{\partial y}\right]+\frac{1}{Fr^2}g_x \tag{23}$$

$$\frac{\partial \tilde{v}}{\partial t}+\frac{\partial uv}{\partial x}+\frac{\partial v^2}{\partial y}=-\frac{\partial \tilde{p}}{\partial y}+\frac{1}{Re}\left[\frac{\partial^2 v}{\partial x^2}+\frac{\partial^2 v}{\partial y^2}+\frac{\partial \Phi^{xy}}{\partial x}+\frac{\partial \Phi^{yy}}{\partial y}\right]+\frac{1}{Fr^2}g_y \tag{24}$$

with $\tilde{\mathbf{u}}(\mathbf{x}, t_n)=\mathbf{u}(\mathbf{x}, t_n)$ using the appropriate boundary conditions for $\tilde{\mathbf{u}}(\mathbf{x}, t)$ at $t=t_n$. Equations (23) and (24) are solved by an explicit finite difference method (essentially Euler's method: it is first order in time and second order in space). It can be shown (see Reference [18])

Copyright © 2006 John Wiley & Sons, Ltd.

DOI: 10.1002/fld

that $\widetilde{\mathbf{u}}(\mathbf{x}, t)$ possesses the correct vorticity at time t. However, $\widetilde{\mathbf{u}}(\mathbf{x}, t)$ does not conserve mass. Let $\mathbf{u}(\mathbf{x}, t)$ be defined by

$$\mathbf{u}(\mathbf{x}, t) - \widetilde{\mathbf{u}}(\mathbf{x}, t) = -\nabla\psi(\mathbf{x}, t) \tag{25}$$

where $\psi(\mathbf{x}, t)$ is a function having the property

$$\nabla^2\psi(\mathbf{x}, t) = \nabla \cdot \widetilde{\mathbf{u}}(\mathbf{x}, t) \tag{26}$$

Thus, $\mathbf{u}(\mathbf{x}, t)$ conserves mass and possesses the correct vorticity at time t. An equation for pressure is obtained as follows. By subtracting (15) from (23) and (16) from (24) we can write

$$\frac{\partial(\mathbf{u} - \widetilde{\mathbf{u}})}{\partial t} = -\nabla(p(\mathbf{x}, t) - \widetilde{p}(\mathbf{x}, t)) \tag{27}$$

Now, introducing (25) into (27), yields

$$-\frac{\partial}{\partial t}\nabla\psi(\mathbf{x}, t) = -\nabla(p(\mathbf{x}, t) - \widetilde{p}(\mathbf{x}, t)) \tag{28}$$

and interchanging the operators in (28) we obtain

$$p(\mathbf{x}, t) = \widetilde{p}(\mathbf{x}, t) + \frac{\partial\psi(\mathbf{x}, t)}{\partial t} \tag{29}$$

which is evaluated as

$$p(\mathbf{x}, t) = \widetilde{p}(\mathbf{x}, t) + \frac{\psi(\mathbf{x}, t)}{\delta t} \tag{30}$$

4. FINITE DIFFERENCE APPROXIMATION

In order to solve Equations (23)–(30) we employ the following finite difference approach.

A staggered grid is used (see Figure 1). The pressure and the rheological functions are positioned at the cell centre while the velocity components are staggered by a factor of $\delta x/2$, $\delta y/2$, respectively. Since the fluid is dynamic, a scheme for identifying the fluid region and the free surface is required. In order to do this, cells of different types need to be introduced: empty cell (E) if the cell contains no fluid; full cell (F) if the cell has fluid and has no face in contact with an empty cell face; surface cell (S) if the cell has fluid and has at least one face in contact with empty cell faces; boundary cell (B) if it is part of a rigid boundary; inflow cell (I) if it defines an inflow boundary; and outflow cell (O) if it is designated as an outflow boundary. Figure 2 illustrates the types of cells that can be present at any one time-step; the empty cells were left blank for clarity.

The momentum equations (23) and (24) are approximated by finite differences as follows. The time derivative is approximated by the explicit Euler method and the linear spatial terms are discretized by central differences. The convective terms are approximated by a high-order upwind method. In this work, we have used the VONOS method (see Reference [19]). Details of the implementation of the Vonos method can be found in Reference [20]. Thus, the intermediate velocity

Copyright © 2006 John Wiley & Sons, Ltd.

DOI: 10.1002/fld

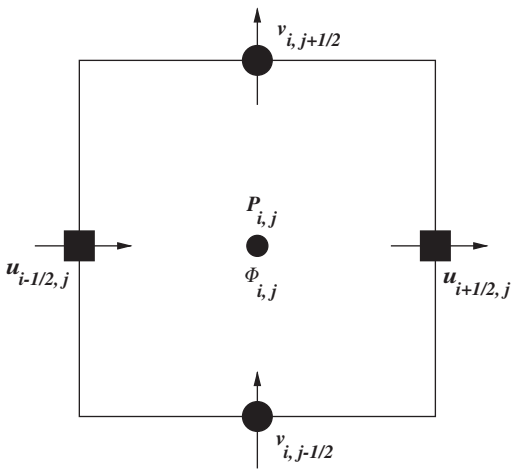

Figure 1. Cell configuration for a second-order fluid flow calculation.

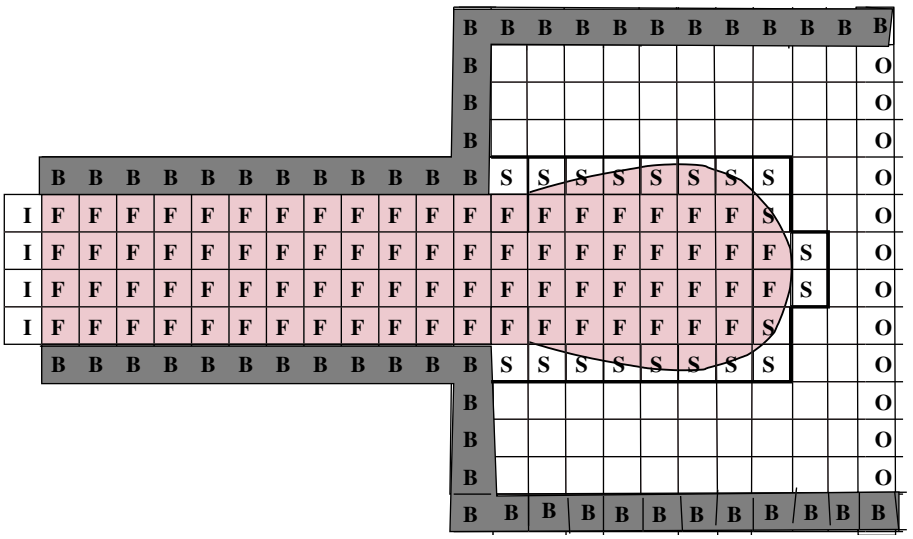

Figure 2. Types of cells within the mesh.

$\tilde{\mathbf{u}}(\mathbf{x}, t)$ is calculated from the discretized equations

$$\tilde{u}_{i+(1/2),j} = u_{i+(1/2),j} + \delta t \left\{ - \mathbf{conv}(uu)|_{i+(1/2),j} - \mathbf{conv}(vu)|_{i+(1/2),j} - \left(\frac{\tilde{p}_{i+1,j} - \tilde{p}_{i,j}}{\delta x} \right) \right.$$

$$\left. + \frac{1}{Re} \left[\left(\frac{u_{i+(3/2),j} - 2u_{i+(1/2),j} + u_{i-(1/2),j}}{\delta x^2} \right) \right. \right.$$

Copyright © 2006 John Wiley & Sons, Ltd.

DOI: 10.1002/fld

$$+\left(\frac{u_{i+(1/2),j+1}-2u_{i+(1/2),j}+u_{i+(1/2),j-1}}{\delta y^2}\right)$$

$$+\frac{\Phi^{xx}_{i+1,j}-\Phi^{xx}_{i,j}}{\delta x}+\frac{\Phi^{xy}_{i+(1/2),j+(1/2)}-\Phi^{xy}_{i+(1/2),j-(1/2)}}{\delta y}\Bigg]+\frac{1}{Fr_2}g_x\Bigg\} \tag{31}$$

$$\widetilde{v}_{i,j+(1/2)}=v_{i,j+(1/2)}+\delta t\left\{-\mathbf{conv}(uv)|_{i,j+(1/2)}-\mathbf{conv}(vv)|_{i,j+(1/2)}-\left(\frac{\widetilde{p}_{i,j+1}-\widetilde{p}_{i,j}}{\delta y}\right)\right.$$

$$+\frac{1}{Re}\left[\left(\frac{v_{i+1,j+(1/2)}-2v_{i,j+(1/2)}+v_{i-1,j+(1/2)}}{\delta x^2}\right)\right.$$

$$+\left(\frac{v_{i,j+(3/2)}-2v_{i,j+(1/2)}+v_{i,j-(1/2)}}{\delta y^2}\right)$$

$$\left.+\frac{\Phi^{xy}_{i+(1/2),j+(1/2)}-\Phi^{xy}_{i-(1/2),j+(1/2)}}{\delta x}+\frac{\Phi^{yy}_{i,j+1}-\Phi^{yy}_{i,j}}{\delta y}\right]+\frac{1}{Fr_2}g_y\Bigg\} \tag{32}$$

where Φ^{xx}, Φ^{xy} and Φ^{yy} are given by (18)–(20), respectively. The operators $\mathbf{conv}(uu)|_{i+(1/2),j}, \ldots,$ $\mathbf{conv}(vv)|_{i,j+(1/2)}$, represent the convective terms of the momentum equations, respectively. The terms $\mathbf{conv}(uD^{xx})|_{i,j}$ and $\mathbf{conv}(vD^{xx})|_{i,j}$ are calculated using the VONOS method (see Reference [19] for details of the VONOS scheme and Reference [20] for details of the finite difference implementation of this high-order upwind method). The definitions of $\mathbf{conv}(uu)|_{i+(1/2),j}$, etc., are rather lengthy and for this reason we refer the reader to Reference [20].

The Poisson equation (26) is discretized at the cell centre using the five point Laplacian which can be written as

$$\psi_{i+1,j}-2\psi_{i,j}+\psi_{i-1,j}+\frac{\delta x^2}{\delta y^2}(\psi_{i,j+1}-2\psi_{i,j}+\psi_{i,j-1})=\delta x^2\widetilde{D}_{i,j} \tag{33}$$

where

$$\widetilde{D}_{i,j}=\frac{\widetilde{u}_{i+(1/2),j}-\widetilde{u}_{i-(1/2),j}}{\delta x}+\frac{\widetilde{v}_{i,j+(1/2)}-\widetilde{v}_{i,j-(1/2)}}{\delta y}$$

The final velocities are obtained by discretizing (25) at the respective nodes, namely

$$u^{n+1}_{i+(1/2),j}=\widetilde{u}_{i+(1/2),j}-\left(\frac{\psi_{i+1,j}-\psi_{i,j}}{\delta x}\right) \tag{34}$$

$$v^{n+1}_{i,j+(1/2)}=\widetilde{v}_{i,j+(1/2)}-\left(\frac{\psi_{i,j+1}-\psi_{i,j}}{\delta y}\right) \tag{35}$$

4.1. Computation of the rheological functions Φ^{xx}, Φ^{xy}, Φ^{yy}

When computing the tilde velocities through (31)–(32) the values of the rheological functions Φ^{xx}, Φ^{xy}, Φ^{yy} are required. They are computed from (18)–(20) as follows.

Copyright © 2006 John Wiley & Sons, Ltd.

DOI: 10.1002/fld

The derivatives $\partial u/\partial x$ and $\partial v/\partial y$ are easily approximated by central differences and are given by

$$\left.\frac{\partial u}{\partial x}\right|_{i,j} = \frac{u_{i+(1/2),j} - u_{i-(1/2),j}}{\delta x}, \quad \left.\frac{\partial v}{\partial y}\right|_{i,j} = \frac{v_{i,j+(1/2)} - v_{i,j-(1/2)}}{\delta y}$$

To compute the cross-derivatives $\partial u/\partial y$ and $\partial v/\partial x$ we first average u and v at the cell faces and then apply central differences, namely

$$\left.\frac{\partial u}{\partial y}\right|_{i,j} = \frac{u_{i,j+(1/2)} - u_{i,j-(1/2)}}{\delta y}, \quad \left.\frac{\partial v}{\partial x}\right|_{i,j} = \frac{v_{i+(1/2),j} - v_{i-(1/2),j}}{\delta x} \tag{36}$$

where

$$u_{i,j+(1/2)} = 0.25(u_{i+(1/2),j} + u_{i-(1/2),j} + u_{i+(1/2),j+1} + u_{i-(1/2),j+1})$$

$$v_{i+(1/2),j} = 0.25(v_{i,j+(1/2)} + v_{i,j-(1/2)} + v_{i+1,j+(1/2)} + v_{i+1,j-(1/2)})$$

with similar expressions for $u_{i,j-(1/2)}$ and $u_{i-(1/2),j}$. However, if the cell (i, j) has one or more faces in contact with an empty cell faces then $\partial v/\partial x$ and $\partial u/\partial y$ are calculated by a forward/backward difference according to which face is in contact with an empty cell face, for instance,

$$\left.\frac{\partial u}{\partial y}\right|_{i,j} = \frac{u_{i,j} - u_{i,j-1}}{\delta y} \quad \text{if the face } (j + \tfrac{1}{2}) \text{ is in contact with an empty cell face}$$

$$\left.\frac{\partial v}{\partial x}\right|_{i,j} = \frac{v_{i,j} - v_{i-1,j}}{\delta x} \quad \text{if the face } (i + \tfrac{1}{2}) \text{ is in contact with an empty cell face}$$

The values of $u_{i,j}$ and $v_{i,j}$ are obtained by averaging, namely,

$$u_{i,j} = 0.5(u_{i+(1/2),j} + u_{i-(1/2),j}), \quad v_{i,j} = 0.5(v_{i,j+(1/2)} + v_{i,j-(1/2)})$$

To approximate the terms contained in the material derivative (D/Dt) we first write them in the form

$$\frac{D(D^{xx})}{Dt} = \frac{\partial D^{xx}}{\partial t} + \mathbf{conv}(uD^{xx}) + \mathbf{conv}(vD^{xx}) \tag{37}$$

with similar expressions for $D(D^{xy})/Dt$ and $D(D^{yy})/Dt$. We shall be investigating flows that possess a steady-state solution and we assume that the contribution from the time derivative in (37) is small. Thus, we employ the approximation

$$\left.\frac{D(D^{xx})}{Dt}\right|_{i,j} \approx \mathbf{conv}(uD^{xx})\big|_{i,j} + \mathbf{conv}(vD^{xx})|_{i,j} \tag{38}$$

The same treatment is applied to $D(D^{xy})/Dt$ and $D(D^{yy})/Dt$. To effect this, it was necessary to compute D^{xx}, D^{xy} and D^{yy} everywhere on the mesh.

Copyright © 2006 John Wiley & Sons, Ltd.

DOI: 10.1002/fld

Therefore, the rheological functions $\Phi^{xx}, \Phi^{xy}, \Phi^{yy}$ can be computed from the following expressions:

$$\Phi^{xx}_{i,j} = -De\left[-\mathbf{conv}(uD^{xx})|_{i,j} - \mathbf{conv}(vD^{xx})|_{i,j} + 4\left(\left.\frac{\partial u}{\partial x}\right|_{i,j}\right)^2 + 2\left.\frac{\partial u}{\partial y}\right|_{i,j}\left(\left.\frac{\partial u}{\partial y}\right|_{i,j} + \left.\frac{\partial v}{\partial x}\right|_{i,j}\right)\right] \tag{39}$$

$$\Phi^{xy} = -2De\left[-\mathbf{conv}(uD^{xy})|_{i,j} - \mathbf{conv}(vD^{xy})|_{i,j} + \left.\frac{\partial u}{\partial x}\right|_{i,j}\left.\frac{\partial v}{\partial x}\right|_{i,j} + \left.\frac{\partial u}{\partial y}\right|_{i,j}\left.\frac{\partial v}{\partial y}\right|_{i,j}\right] \tag{40}$$

$$\Phi^{yy} = -De\left[-\mathbf{conv}(uD^{yy})|_{i,j} - \mathbf{conv}(vD^{yy})|_{i,j} + 4\left(\left.\frac{\partial v}{\partial y}\right|_{i,j}\right)^2 + 2\left.\frac{\partial v}{\partial x}\right|_{i,j}\left(\left.\frac{\partial u}{\partial y}\right|_{i,j} + \left.\frac{\partial v}{\partial x}\right|_{i,j}\right)\right] \tag{41}$$

4.2. Finite difference approximation of the free surface stress conditions

Let $\mathbf{n} = (n_x, n_y)$ and $\mathbf{m} = (n_y, -n_x)$ denote unit normal and tangential vectors to the free surface, respectively. Then, the stress conditions (5) can be written as

$$p - \frac{1}{Re}[(D^{xx} + \Phi^{xx})n_x^2 + (D^{yy} + \Phi^{yy})n_y^2 + 2(D^{xy} + \Phi^{xy})n_x n_y] = 0 \tag{42}$$

$$\frac{2}{Re}[(D^{xx} - D^{yy} + \Phi^{xx} - \Phi^{yy})n_x\, n_y + (D^{xy} + \Phi^{xy})(n_x^2 - n_y^2)] = 0 \tag{43}$$

We point out that the problems we intend to solve have low Reynolds numbers, and therefore when applying the conditions above we shall neglect the convective terms from the material derivative appearing in the computation of the rheological functions $\Phi^{xx}, \Phi^{xy}, \Phi^{yy}$. In order to apply these conditions we follow the ideas adopted by Tome *et al.* [18]. We suppose the mesh spacing is sufficiently small so that the free surface can be represented, locally, by a linear surface which is either parallel to one coordinate axis or is at an angle of 45° to it. In this case, conditions (42) and (43) are applied as follows.

(i) *Surface cells* (S) *having only one face in contact with an empty cell* (E) *face*. In these cells we assume that the free surface is either horizontal or vertical according to which face is in contact with the E-cell. In either of these cases, the normal vector can be written as $\mathbf{n} = (\pm 1, 0)$ or $\mathbf{n} = (0, \pm 1)$. For instance, if we consider the S-cell shown in Figure 3 we take $\mathbf{n} = (1, 0)$ and

Copyright © 2006 John Wiley & Sons, Ltd.

DOI: 10.1002/fld

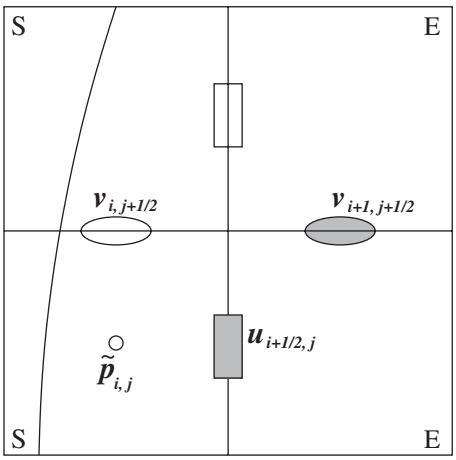

Figure 3. Surface cell having the $(i+\frac{1}{2})$-face in contact with one empty cell face.

Equations (42) and (43) reduce to

$$\tilde{p} + \frac{1}{Re}(D^{xx} + \Phi^{xx}) = 0 \tag{44}$$

$$\frac{1}{Re}(D^{xy} + \Phi^{xy}) = 0 \tag{45}$$

respectively.

We observe that when computing the velocity $\tilde{v}_{i,j+(1/2)}$ in Figure 3, the values of $\tilde{p}_{i,j}$, $u_{i+(1/2),j}$ and $v_{i+1,j+(1/2)}$ are required. They are obtained as follows. First we calculate $u_{i+(1/2),j}$ by applying the mass conservation equation at the centre of the surface cell which gives

$$u_{i+(1/2),j} = u_{i-(1/2),j} + \frac{\delta x}{\delta y}(v_{i,j+(1/2)} - v_{i,j-(1/2)}) \tag{46}$$

The value of $v_{i+1,j+(1/2)}$ is then computed by approximating (45) at the cell corner $(i+\frac{1}{2}, j+\frac{1}{2})$ which can be written as

$$\frac{u_{i+(1/2),j+1} - u_{i+(1/2),j}}{\delta y} + \frac{v_{i+1,j+(1/2)} - v_{i,j+(1/2)}}{\delta x}$$
$$- 2De\left(\frac{v_{i+1,j+(1/2)} - v_{i,j+(1/2)}}{\delta x} \frac{\partial u}{\partial x}\bigg|_{i+(1/2),j+(1/2)} \right.$$
$$\left. + \frac{u_{i+(1/2),j+1} - u_{i+(1/2),j}}{\delta y} \frac{\partial v}{\partial y}\bigg|_{i+(1/2),j+(1/2)} \right) = 0 \tag{47}$$

Copyright © 2006 John Wiley & Sons, Ltd.

DOI: 10.1002/fld

or

$$v_{i+1,j+(1/2)} = v_{i,j+(1/2)} - \delta x \left.\frac{\partial u}{\partial y}\right|_{i+\frac{1}{2},j+\frac{1}{2}} \frac{\left(1 - 2De \left.\dfrac{\partial v}{\partial y}\right|_{i+\frac{1}{2},j+\frac{1}{2}}\right)}{\left(1 - 2De \left.\dfrac{\partial u}{\partial x}\right|_{i+\frac{1}{2},j+\frac{1}{2}}\right)} \tag{48}$$

The derivative $\partial u/\partial x|_{i+(1/2),j+(1/2)}$ is evaluated by using backward differences while the derivative $\partial v/\partial y|_{i+(1/2),j+(1/2)}$ is approximated by central differences at $(i, j+\frac{1}{2})$. The pressure $\widetilde{p}_{i,j}$ is calculated using (44) applied at the cell centre giving

$$\widetilde{p}_{i,j} = \frac{1}{Re}(D^{xx}_{i,j} + \Phi^{xx}_{i,j}) \tag{49}$$

Other configurations of surface cells having only one face in contact with an empty cell face are handled similarly.

(ii) *Surface cells* (S) *having two adjacent faces in contact with empty cell* (E) *faces.* For these cells we assume the free surface is 45° sloped between the coordinate axes. Thus, on these surfaces the normal vector takes the form $\mathbf{n} = (\pm(\sqrt{2}/2), \pm(\sqrt{2}/2))$. For instance, if consider the surface cell shown in Figure 4 we take $\mathbf{n} = (\sqrt{2}/2, \sqrt{2}/2)$. In this case, it can be shown that conditions (42) and (43) may be written as

$$\widetilde{p} = \frac{1}{2Re}(D^{xy}_{i,j} + \Phi^{xx} + \Phi^{yy} + \Phi^{xy}) \tag{50}$$

$$\frac{\partial v}{\partial y} - \frac{\partial u}{\partial x} + De\left(\frac{\partial u}{\partial y}\right)^2 - De\left(\frac{\partial v}{\partial x}\right)^2 = 0 \tag{51}$$

where the convective terms in the rheological functions have been assumed to be negligible.

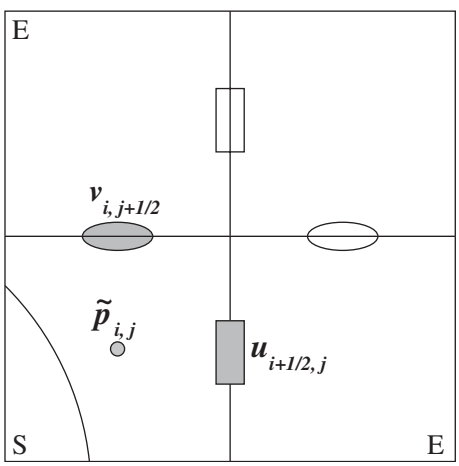

Figure 4. Surface cell having the $(i+\frac{1}{2})$ and the $(j+\frac{1}{2})$-faces in contact with empty cell faces.

Copyright © 2006 John Wiley & Sons, Ltd.

DOI: 10.1002/fld

The velocities $u_{i+(1/2),j}$, $v_{i,j+(1/2)}$ and the pressure $\widetilde{p}_{i,j}$ in Figure 4 are calculated by using Equations (50), (51) and the mass conservation equation applied at the cell centre as follows. Equation (51) can be approximated by

$$\begin{aligned}
&\frac{v_{i,j+(1/2)} - v_{i,j-(1/2)}}{\delta y} - \frac{u_{i+(1/2),j} - u_{i-(1/2),j}}{\delta x} \\
&+ De \left\{ \left(\frac{1}{2} \frac{u_{i+(1/2),j} + u_{i-(1/2),j} - u_{i+(1/2),j-1} - u_{i-(1/2),j-1}}{\delta y} \right)^2 \right. \\
&\left. - \left(\frac{1}{2} \frac{v_{i,j+(1/2)} + v_{i,j-(1/2)} - v_{i-1,j+(1/2)} - v_{i-1,j-(1/2)}}{\delta x} \right)^2 \right\} = 0
\end{aligned} \tag{52}$$

Equation (52) and the mass conservation (46) provides a 2×2-system for the unknowns $u_{i+(1/2),j}$ and $v_{i,j+(1/2)}$. This system can be solved as follows. First, by introducing $u_{i+(1/2),j}$ from (46) into (52) we obtain

$$\begin{aligned}
&2v_{i,j+(1/2)} - 2v_{i,j-(1/2)} + \frac{De}{4} \left\{ \frac{1}{\delta y} \left[\frac{\delta x^2}{\delta y^2} v_{i,j+(1/2)}^2 \right. \right. \\
&+ 2\frac{\delta x}{\delta y} v_{i+(1/2)} \left(2u_{i-(1/2),j} + \frac{\delta x}{\delta y} v_{i,j-(1/2)} - u_{i+(1/2),j-1} - u_{i-(1/2),j-1} \right) \\
&\left. + \left(2u_{i-(1/2),j} + \frac{\delta x}{\delta y} v_{i,j-(1/2)} - u_{i+(1/2),j-1} - u_{i-(1/2),j-1} \right)^2 \right] \\
&- \frac{\delta y}{\delta x^2} \left[v_{i,j+(1/2)}^2 + 2v_{i,j+(1/2)} \left(v_{i,j-(1/2)} - v_{i-1,j+(1/2)} - v_{i-1,j-(1/2)} \right) \right. \\
&\left. \left. + \left(v_{i,j-(1/2)} - v_{i-1,j+(1/2)} - v_{i-1,j-(1/2)} \right)^2 \right] \right\} = 0
\end{aligned} \tag{53}$$

It can be seen that Equation (53) provides two solutions for $v_{i,j+(1/2)}$. However, if $\delta x = \delta y = h$ then the quadratic term vanishes and it can be shown that in this case $v_{i,j+(1/2)}$ is uniquely determined and is given by

$$\begin{aligned}
&v_{i,j+(1/2)} \\
&= \frac{-v_{i,j-(1/2)} - \frac{De}{8h} \left[(2u_{i-(1/2),j} - u_{i+(1/2),j-1} - u_{i-(1/2),j-1} + v_{i-(1/2)})^2 + (v_{i,j-(1/2)} - v_{i-1,j+(1/2)} - v_{i-1,j-(1/2)})^2 \right]}{1 + \frac{De}{4h} \left[2u_{i-(1/2),j} + v_{i-(1/2)} - u_{i+(1/2),j-1} - u_{i-(1/2),j-1} + v_{i,j-(1/2)} - v_{i-1,j+(1/2)} - v_{i-1,j-(1/2)} \right]}
\end{aligned} \tag{54}$$

After computing $v_{i,j+(1/2)}$ using (54), the value of $u_{i+(1/2),j}$ is obtained from the continuity equation. The pressure at the surface cell centre is then computed from (50), namely,

$$\widetilde{p}_{i,j} = \frac{1}{2Re} (D_{i,j}^{xy} + \Phi_{i,j}^{xx} + \Phi_{i,j}^{yy} + \Phi_{i,j}^{xy}) \tag{55}$$

Copyright © 2006 John Wiley & Sons, Ltd.

DOI: 10.1002/fld

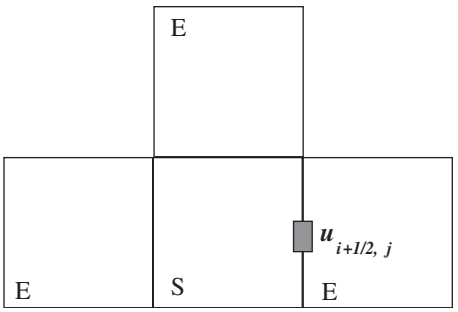

Figure 5. Surface cell having three faces in contact with empty cell faces.

Other configurations of surface cells having two adjacent faces in contact with empty cell faces are treated similarly.

(iii) *Surface cells* (S) *having two opposite faces in contact with empty cell* (E) *faces*. These cells do not provide enough information to obtain an approximation for the normal vector. In these cells we set the pressure equal to zero and use the mass conservation equation to adjust one velocity. For instance, if the surface cell has three faces in contact with empty cell faces (see Figure 5) we set $\widetilde{p}_{i,j}=0$ and (in the case when $\delta x=\delta y$) $u_{i+(1/2),j}=u_{i-(1/2),j}-v_{i,j+(1/2)}+v_{i,j-(1/2)}$.

4.3. Time-step control and particle movement

A time-step procedure for calculating the time-step size for every calculational cycle is employed. This procedure was presented by Tome and McKee [21] for Newtonian flows and is based on the stability restrictions

$$\delta t_1 < \max\left\{\frac{\delta x}{U_{\max}}, \frac{\delta y}{V_{\max}}\right\}, \quad \delta t_2 < \frac{\delta x^2}{4} Re \quad \text{(here again it is assumed that } \delta x=\delta y\text{)}$$
$$\delta t = \text{FACT}\min(\delta t_1, \delta t_2) \quad \text{where } 0<\text{FACT}<1 \tag{56}$$

where $U_{\max}=\max\{|u|\}$ and $V_{\max}=\max\{|v|\}$. The factor FACT is employed as a conservative measure to allow for the fact that the stability analysis has been performed locally and the values of $U_{\max}$ and $V_{\max}$ are not known *a priori*, that is, mass conservation has not yet been satisfied. Further, details of the implementation of this time-step procedure can be found in Reference [21]. Usually, when simulating Newtonian flows the factor FACT takes the value of 0.5. However, for second-order fluid flow simulations a more restrictive value is used depending on the value of the Deborah number De. In the results presented in this paper we used a value of 0.1 for the factor FACT.

Once the mass conserved velocities have been calculated the last step of the numerical method described in Section 3 is to update the marker particle positions. The new markers positions are obtained by solving

$$\frac{\mathrm{d}\mathbf{x}_p}{\mathrm{d}t}=\mathbf{u}_p \tag{57}$$

Copyright © 2006 John Wiley & Sons, Ltd.

DOI: 10.1002/fld

for each particle by using the explicit Euler method. The particle velocity $\mathbf{u}_p$ is found by performing a bilinear interpolation using the nearest four node velocities. Details of the particle movement can be found in Reference [21].

5. CHANNEL FLOW

The finite difference equations described in Section 4 have been implemented into the FreeFlow-2D code in order to simulate flows of a second-order fluid. In this section, we present results to partially validate the numerical method.

5.1. Validation

We validate the numerical method presented in this paper by simulating the flow in a two-dimensional channel. We consider a channel having an entrance with width L and a length $15L$ (see Figure 6). At the channel entrance we prescribe a fully developed flow defined by

$$u(y) = -4\frac{U}{L^2}\left(y - \frac{L}{2}\right)^2 + U, \quad v = 0, \quad 0 \leqslant y \leqslant L \tag{58}$$

On the channel walls the velocity field satisfies the no-slip condition while at the outflow Neumann conditions are assumed. Initially, the channel is empty and fluid is injected at the inflow until the channel is full and steady state has been reached. It can be seen that under fully developed flow conditions, the components of the extra-stress tensor (see Equations (17)) reduce to

$$\tau^{xx} = -\frac{2De}{Re}\left(\frac{\partial u}{\partial y}\right)^2, \quad \tau^{xy} = \frac{1}{Re}\left(\frac{\partial u}{\partial y}\right), \quad \tau^{yy} = 0 \tag{59}$$

We point out that under steady state Equations (58) and (59) are valid throughout the channel.

To simulate this problem we used the following input data: $L = 1\,\text{cm}$, $U = 1\,\text{ms}^{-1}$ and gravity was neglected ($g_x = g_y = 0$). The material properties were $\nu_0 = \eta_0/\rho = 0.01\,\text{m}^2\,\text{s}^{-1}$ and $\lambda_2 = 0.0045\,\text{s}$. The scaling parameters were chosen to be L, U and ν_0 so that $Re = UL/\nu_0 = 1$ and $De = \lambda_2 U/L = 0.45$. To demonstrate the convergence of the numerical method we ran this problem using three meshes: **Mesh1**—$\delta x = \delta y = 0.125\,\text{cm}$ (8×120 cells); **Mesh2**—$\delta x = \delta y = 0.0625\,\text{cm}$ (16×240 cells); and **Mesh3**—$\delta x = \delta y = 0.03125\,\text{cm}$ (32×480 cells). All the three runs achieved steady state. The time evolution of the streamlines of the u-velocity obtained using **Mesh3** is shown in Figure 7. Figures 8 and 9 display the values of the extra-stress components τ^{xx} and τ^{xy} at different times.

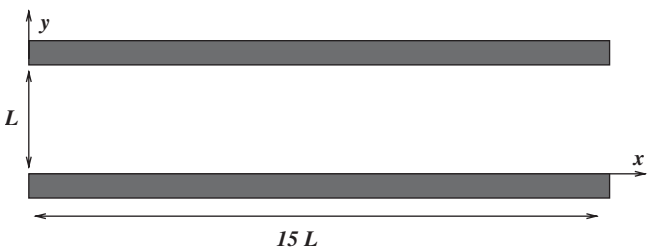

Figure 6. Domain description for the channel flow simulation.

Copyright © 2006 John Wiley & Sons, Ltd.

DOI: 10.1002/fld

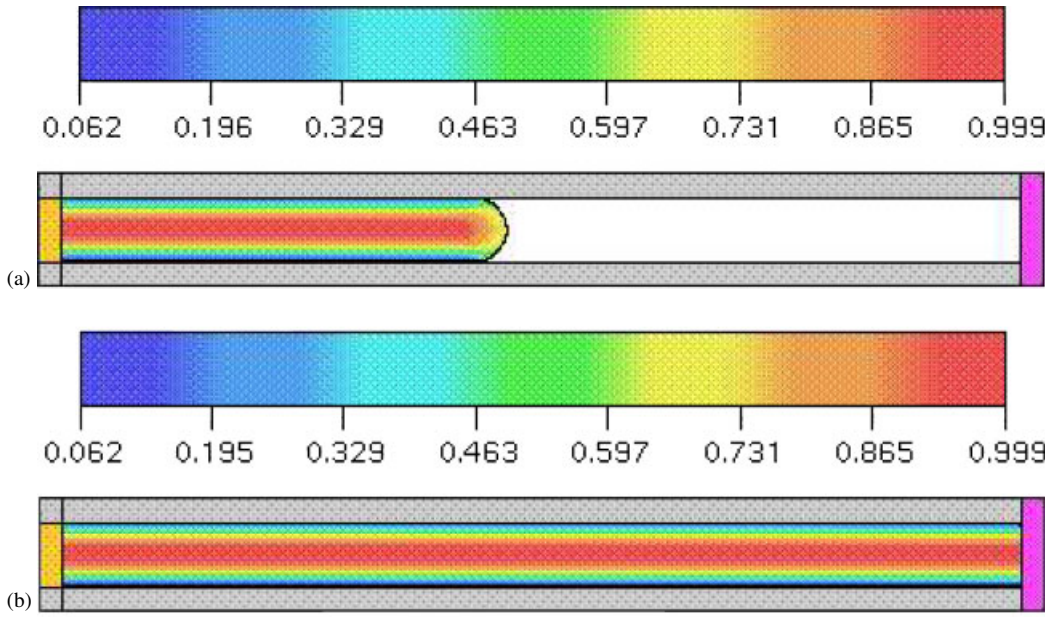

Figure 7. Contour lines for the velocity u: (a) $t = 0.1$ s; and (b) $t = 0.545$ s.

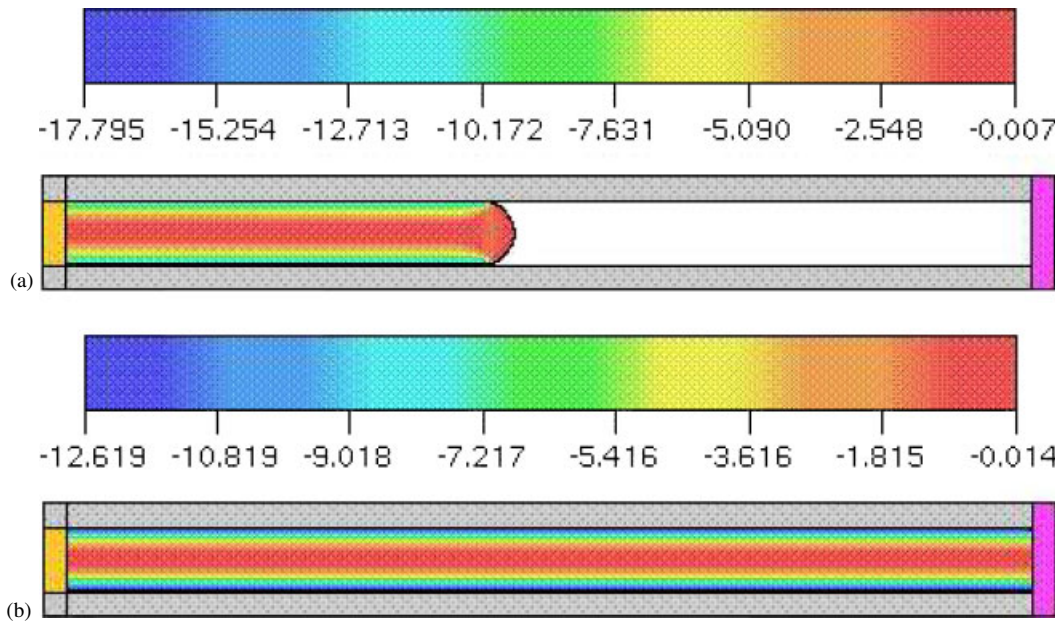

Figure 8. Contour lines of τ^{xx}: (a) $t = 0.1$ s; and (b) $t = 0.545$ s.

Copyright © 2006 John Wiley & Sons, Ltd.

DOI: 10.1002/fld

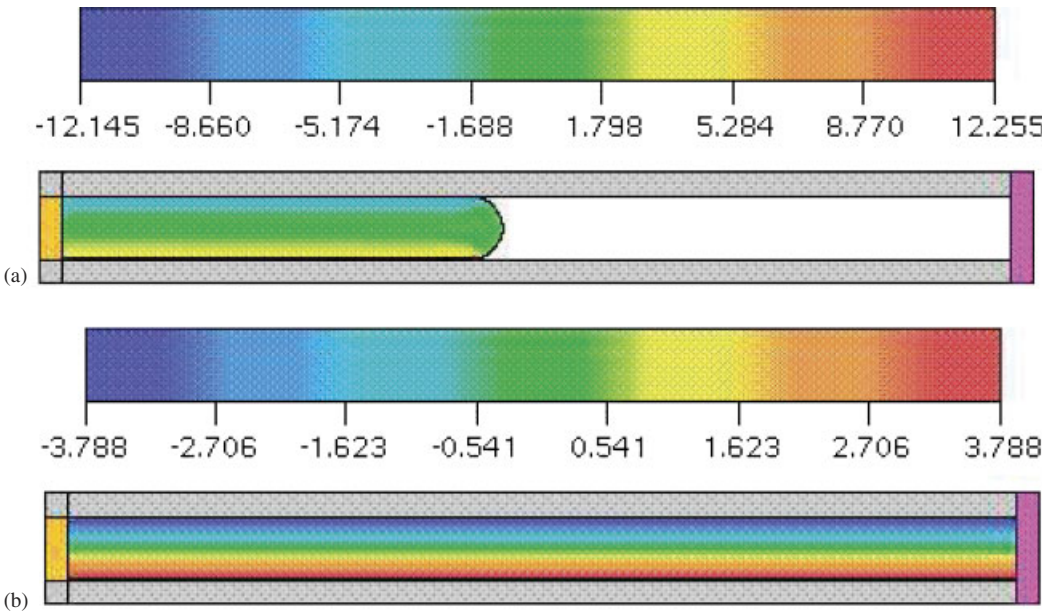

Figure 9. Contour lines of τ^{xy}: (a) $t = 0.1$ s; and (b) $t = 0.545$ s.

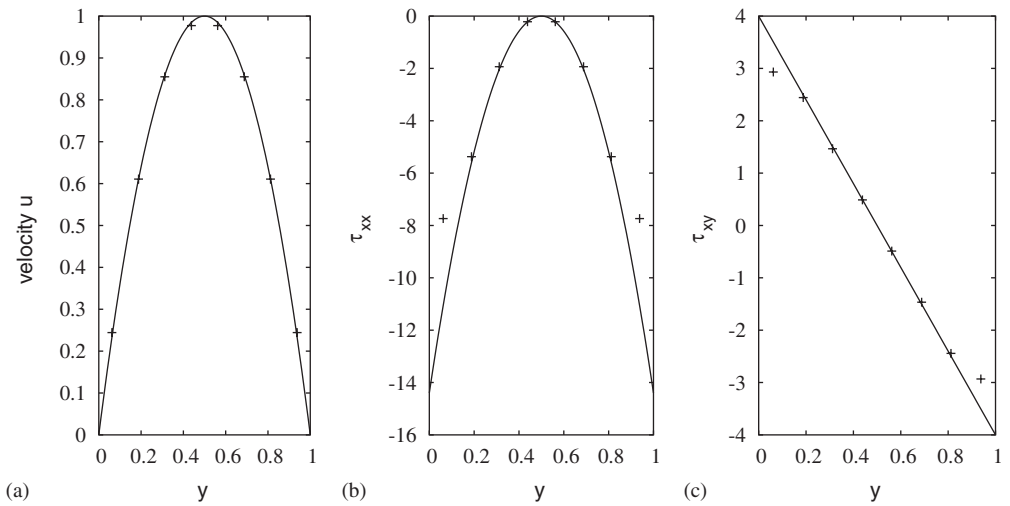

Figure 10. Numerical simulation of the channel flow with $Re = 1$ and $De = 0.45$ (symbols) using **Mesh1**. Comparison with analytic solutions (solid lines): (a) velocity u; (b) extra-stress component τ^{xx}; and (c) extra-stress component τ^{xy}. Results shown at position $x = 7.5$ cm.

We can see in Figure 7(b) that the streamlines are all parallel indicating that the steady state has been reached. Figure 10 shows the results obtained for the extra-stress components τ^{xx} and τ^{xy} and the velocity component u at the middle of the channel ($x = 7.5$) using **Mesh1**

Copyright © 2006 John Wiley & Sons, Ltd.

DOI: 10.1002/fld

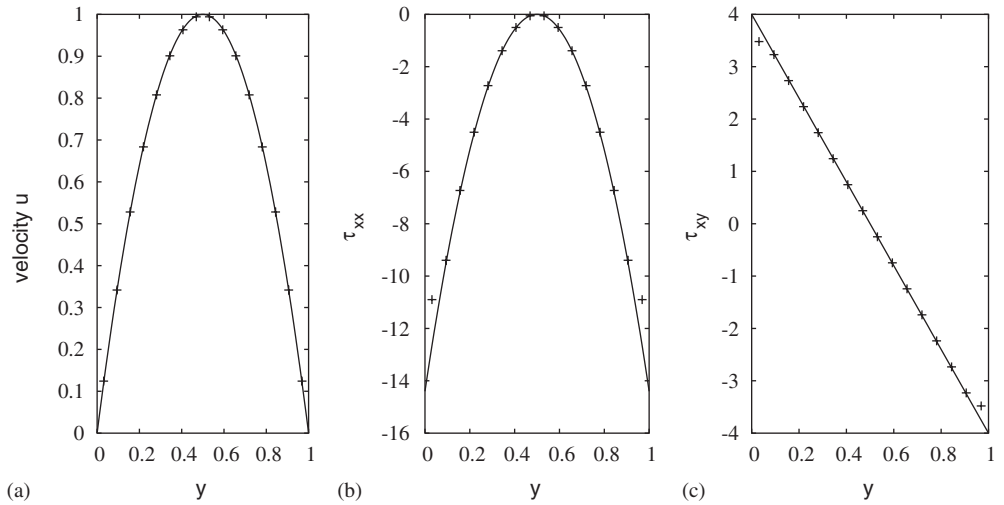

Figure 11. Numerical simulation of the channel flow with $Re = 1$ and $De = 0.45$ (symbols) using **Mesh2**. Comparison with analytic solutions (solid lines): (a) velocity u; (b) extra-stress component τ^{xx}; and (c) extra-stress component τ^{xy}. Results shown at position $x = 7.5$ cm.

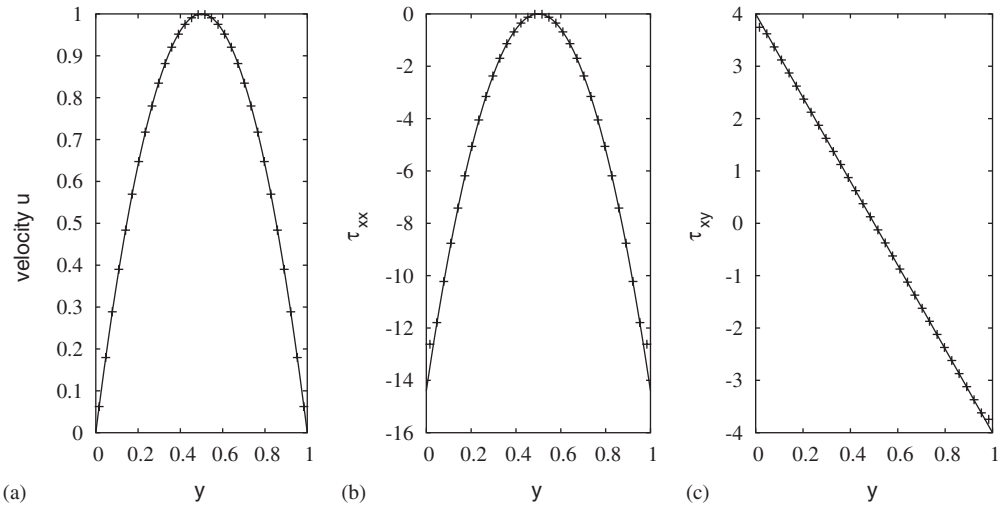

Figure 12. Numerical simulation of the channel flow with $Re = 1$ and $De = 0.45$ (symbols) using **Mesh3**. Comparison with analytic solutions (solid lines): (a) velocity u; (b) extra-stress component τ^{xx}; and (c) extra-stress component τ^{xy}. Results shown at position $x = 7.5$ cm.

and Figure 11 displays similar results obtained on **Mesh2**. The three results using **Mesh3** are displayed in Figure 12. As we can see in Figures 10–12, the agreement between the numerical results and the exact solution for the velocity field on all the three meshes is good. However, the numerical results for the extra-stress components τ^{xx} and τ^{xy} near the channel walls using **Mesh1**

Copyright © 2006 John Wiley & Sons, Ltd.

DOI: 10.1002/fld

Table I. Channel flow simulation: l_2-errors of τ^{xx} and τ^{xy} using the three meshes.

	Mesh1	**Mesh2**	**Mesh3**
$E(\tau^{xx})$	6.92×10^{-2}	9.52×10^{-3}	1.22×10^{-3}
$E(\tau^{xy})$	1.56×10^{-2}	1.74×10^{-3}	2.02×10^{-4}

do not agree very well with the exact solutions. Nonetheless, as the mesh is refined (see Figures 11 and 12) we observe that the numerical results approach their appropriate exact solutions. This indicates that, for this simple flow field at least, the numerical method described in this paper does indeed converge. To further demonstrate the convergence of the numerical method we computed the relative l_2-norm of the errors

$$E(\tau^{xx}) = \frac{\sum(\tau^{xx} - \tau^{xx}_{\text{numer}})^2}{\sum \tau^{xx}}, \quad E(\tau^{xy}) = \frac{\sum(\tau^{xy} - \tau^{xy}_{\text{numer}})^2}{\sum \tau^{xy}} \tag{60}$$

using the results obtained on the three meshes. Table I displays the values of the relative errors on the three meshes and it can be seen that the relative errors decrease as the mesh is refined. Thus, these results demonstrate the convergence of the numerical method for flow in a channel.

6. NUMERICAL SIMULATIONS

In this section, we perform two numerical simulations that display viscoelastic behaviour: flow through a planar 4:1 contraction and extrudate swell.

6.1. Numerical simulation of flow through a planar 4:1 contraction

We considered the flow of a second-order fluid through a planar 4:1 contraction. A schematic diagram of this geometry is displayed in Figure 13. At the fluid entrance we imposed parabolic Poiseuille flow and assumed that the exit of the narrow channel was sufficiently far downstream so that the flow was parabolic at the outflow. On the contraction walls the velocity field obeys the no-slip condition.

To simulate this problem the following input data were employed (Figure 14).

Mesh size: $L = 1\,\text{cm}$ and $\delta x = \delta y = 0.125\,\text{cm}$, giving 240×64 cells within the mesh;

Scaling parameters: $U = 1\,\text{ms}^{-1}$, $L = 1\,\text{cm}$, Poisson solver tolerance: $\varepsilon = 10^{-10}$ (see Reference [21]).

The kinematic viscosity of the fluid was assigned the values of $\nu = 1.0$ and $\nu = 0.1$ so that this problem was solved for Reynolds numbers $Re = 0.1$ and $Re = 1$. Furthermore, since we were interested in observing viscoelastic behaviour we varied the Deborah number by setting the values of the temporal constant λ_2 to 0.0, 0.4, 0.8, 1.2 and 1.4; the constant λ_4 was set to zero in all of these runs. Consequently, the flow was simulated for Deborah numbers $De = \lambda_2 U/L$ of 0.0 (Newtonian case), 0.4, 0.8, 1.2 and 1.4, respectively. The results obtained with $Re = 0.1$ are shown in Figure 15 while the results with $Re = 1$ are displayed in Figure 16. We observe in Figures 15 and 16 that, as the Deborah number is increased, so the size of the corner vortex decreased; these results agree qualitatively with those obtained, for instance, by Phillips and Williams [5] and Sato and Richardson [8] for the Oldroyd-B model. The results for the case of $De = 1.4$ are shown in

Copyright © 2006 John Wiley & Sons, Ltd.

DOI: 10.1002/fld

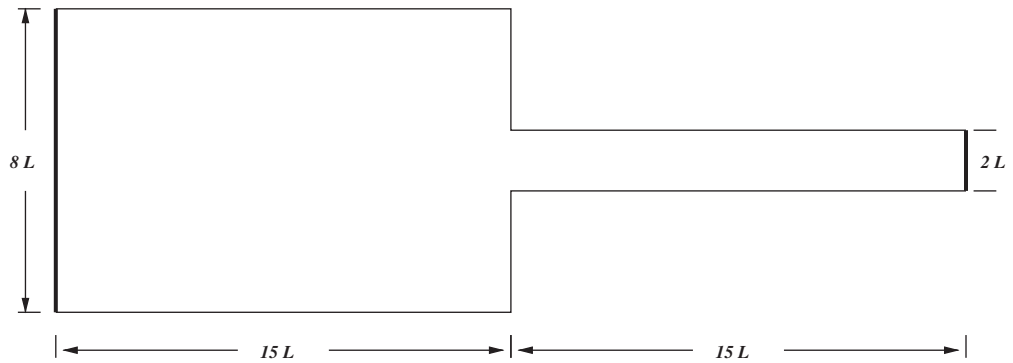

Figure 13. Geometry of the planar 4:1 contraction problem.

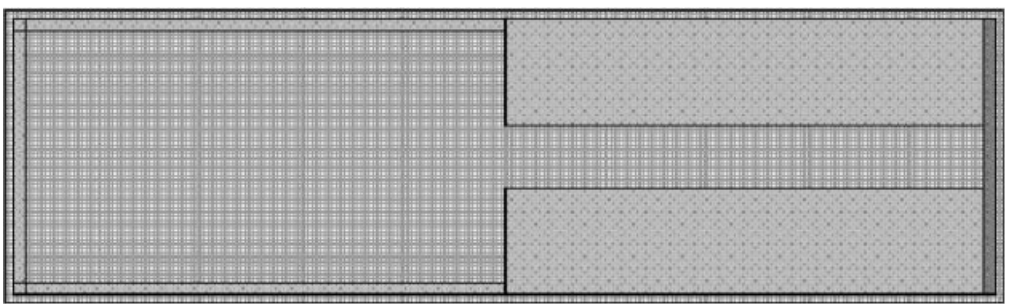

Figure 14. Mesh employed for the planar 4:1 contraction problem.

Figure 17 and it is observed that the streamlines in the downstream channel have some wiggles, which would appear to suggest that convergence to the steady state had not been achieved. This would appear to point to an upper limit for the Deborah number for the numerical method, at least when applied to contraction flow.

6.2. Numerical simulation of the extrudate swell of a second-order fluid

The flow produced by a jet as it emerges from a die has practical industrial importance and has been studied experimentally and numerically by many authors. For example, Tanner [22] (see also Reference [23]) presented a theory based on the KBKZ constitutive model for predicting swelling ratios. Various authors have numerically studied extrudate swell: Crochet and Keunings [24], Caswell and Viriyayuthakorn [25], Ngamaramvaranggul and Webster [26], have employed the Maxwell model while the Oldroyd-B model has been used by other researchers (e.g. References [11, 12, 26–29]). In particular, Crochet and Keunings [11] computed the extrudate swell of planar and axisymmetric Oldroyd-B jets while a detailed study of circular jet swelling for a large range of relaxation ratios was presented by Bush [29]. Much less has been done using the CEF model. However, Gast and Ellingson [13] computed the extrudate swell of a second-order fluid. They employed the commercial finite element code Fidap [14] and obtained results on the extrudate swell in tubular dies. It would appear that the code FIDAP could not cope with high elastic fluids since their results were limited to swellings up to 24%.

Copyright © 2006 John Wiley & Sons, Ltd.

DOI: 10.1002/fld

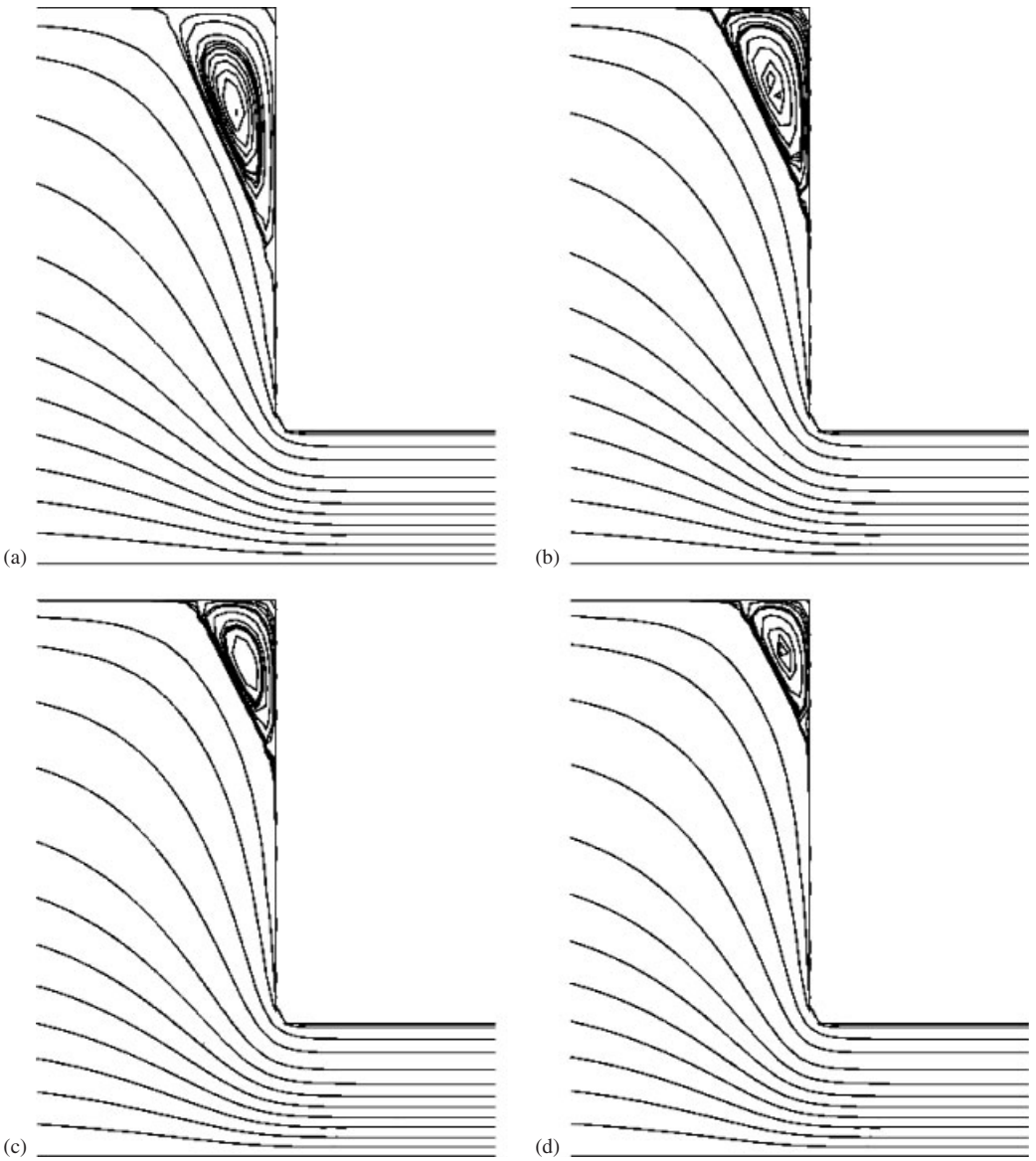

Figure 15. Numerical simulation of the flow through a 4:1 contraction. Streamlines for the case $Re = 0.1$: (a) $De = 0$; (b) $De = 0.4$; (c) $De = 0.8$; and (d) $De = 1.2$.

To demonstrate that the numerical method presented in this paper can cope with high elastic fluids governed by the second-order fluid constitutive equation (3) we performed several simulations of the extrudate swell with increasing Deborah numbers. The input data describing the computational domain are displayed in Figure 18. On the channel walls the velocity field obeys the no-slip condition while on the free surface the stress conditions (see Equations (42) and (43)) are imposed

Copyright © 2006 John Wiley & Sons, Ltd.

DOI: 10.1002/fld

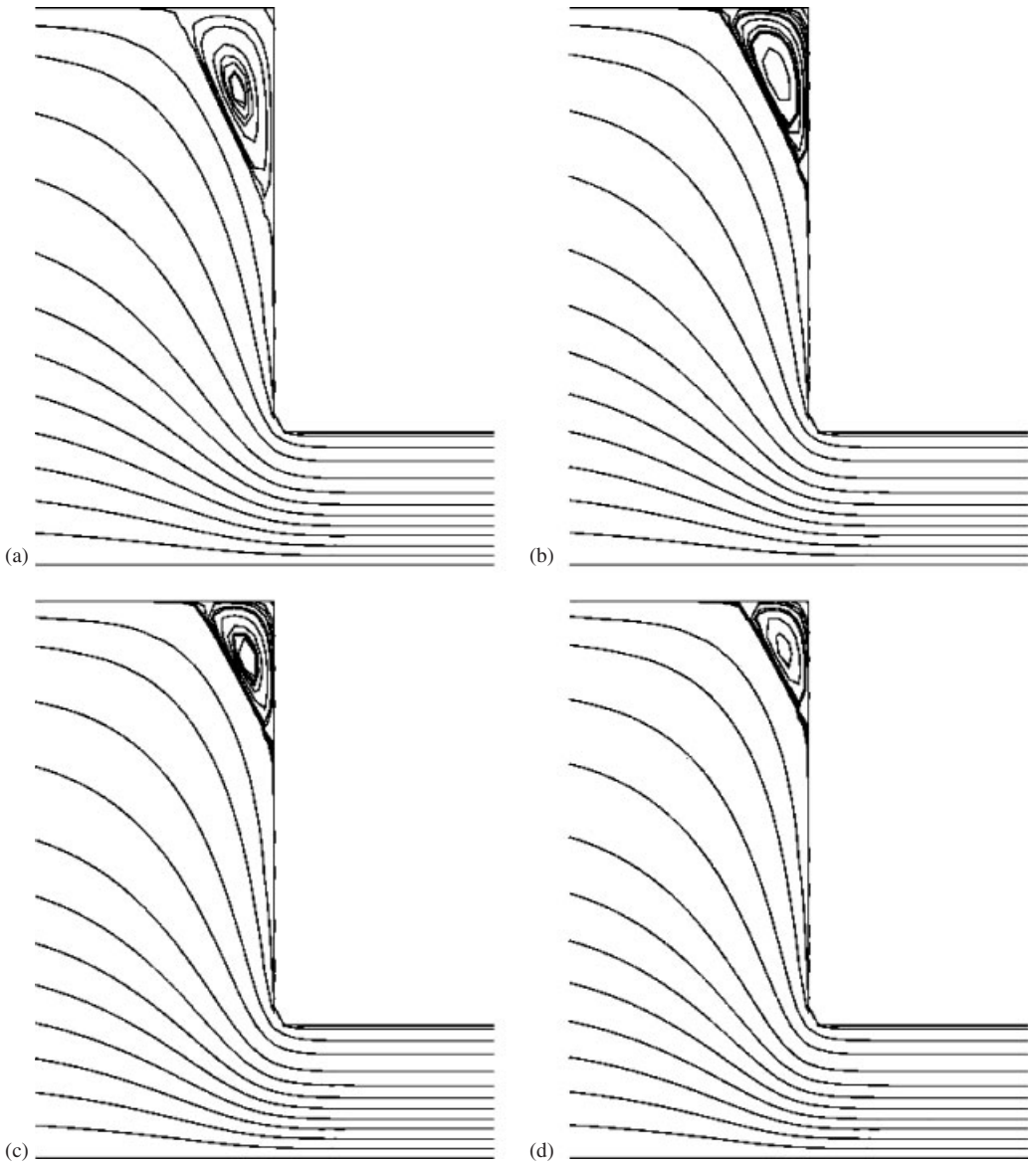

Figure 16. Numerical simulation of the flow through a 4:1 contraction. Streamlines for the case $Re = 1$: (a) $De = 0$; (b) $De = 0.4$; (c) $De = 0.8$; and (d) $De = 1.2$.

according to the treatment given in Section 4.2. At the fluid entrance the velocity is prescribed by a parabolic profile given by Equation (58) where $U = 1\,\mathrm{ms}^{-1}$ and the channel width was $D = 1\,\mathrm{cm}$ (see Figure 18). The domain size was $15\,\mathrm{cm} \times 3\,\mathrm{cm}$ and a mesh size of $\delta x = \delta y = 0.0625\,\mathrm{cm}$ (208×48 cells within the domain) was employed. Gravity was neglected and the value of the kinematic viscosity was taken to be $v_0 = 0.01\,\mathrm{m}^2\,\mathrm{s}^{-1}$. The retarded-motion constant λ_2 was taken to

Copyright © 2006 John Wiley & Sons, Ltd.

DOI: 10.1002/fld

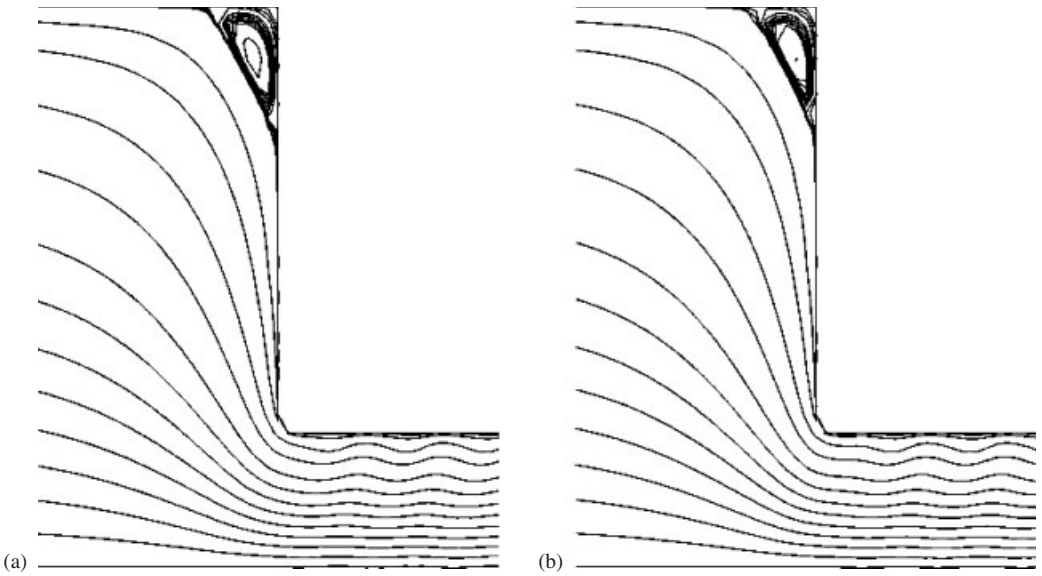

Figure 17. Numerical simulation of the flow through a 4:1 contraction. Streamlines for the case $De = 1.4$: (a) $Re = 0.1$; and (b) $Re = 1$.

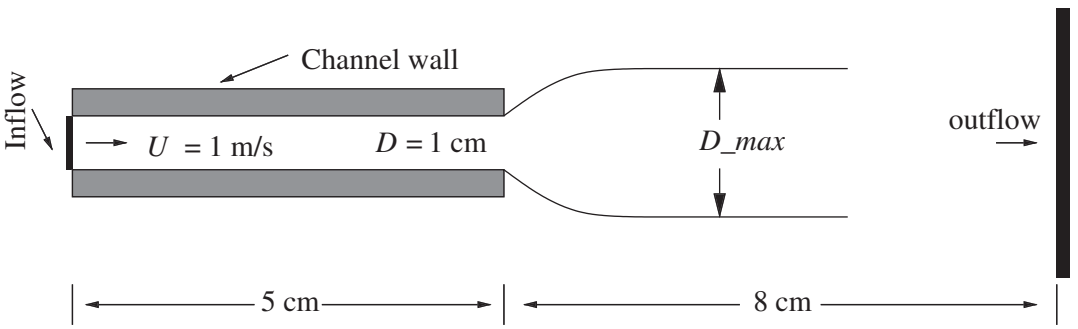

Figure 18. Domain specification for the simulation of the extrudate swell of a second-order fluid.

be 0.001, 0.002, 0.003, 0.004, 0.005, 0.006, 0.007 and 0.008 s. The scaling parameters were U, D, v_0 and λ_2; consequently, $Re = 1$ and the Deborah numbers were $De = 0.1, 0.2, 0.3, 0.4, 0.5, 0.6, 0.7$ and 0.8, respectively. We point out that for the case of $De = 0.8$ our numerical method did not converge and wiggles, similar to those obtained for $De = 1.4$ on the 4:1 planar contraction flow simulation, appeared inside the channel. However, using a coarse mesh of $\delta x = \delta y = 0.1$ cm (130×30 cells within the domain) the simulation of the extrudate swell did appear to lose its oscillating behaviour. This would seem to suggest that there is an upper Deborah number limit beyond which convergence is not achieved. The results of these simulations for the cases of $De = 0.2, 0.4, 0.6$ and 0.8 are displayed in Figures 19–22, respectively. We point out that for $De = 0.2$ the swelling ratio $S_r = D_{\max}/D$ (see Figure 18) was 1.43 while for $De = 0.8$ we obtained

Copyright © 2006 John Wiley & Sons, Ltd.

DOI: 10.1002/fld

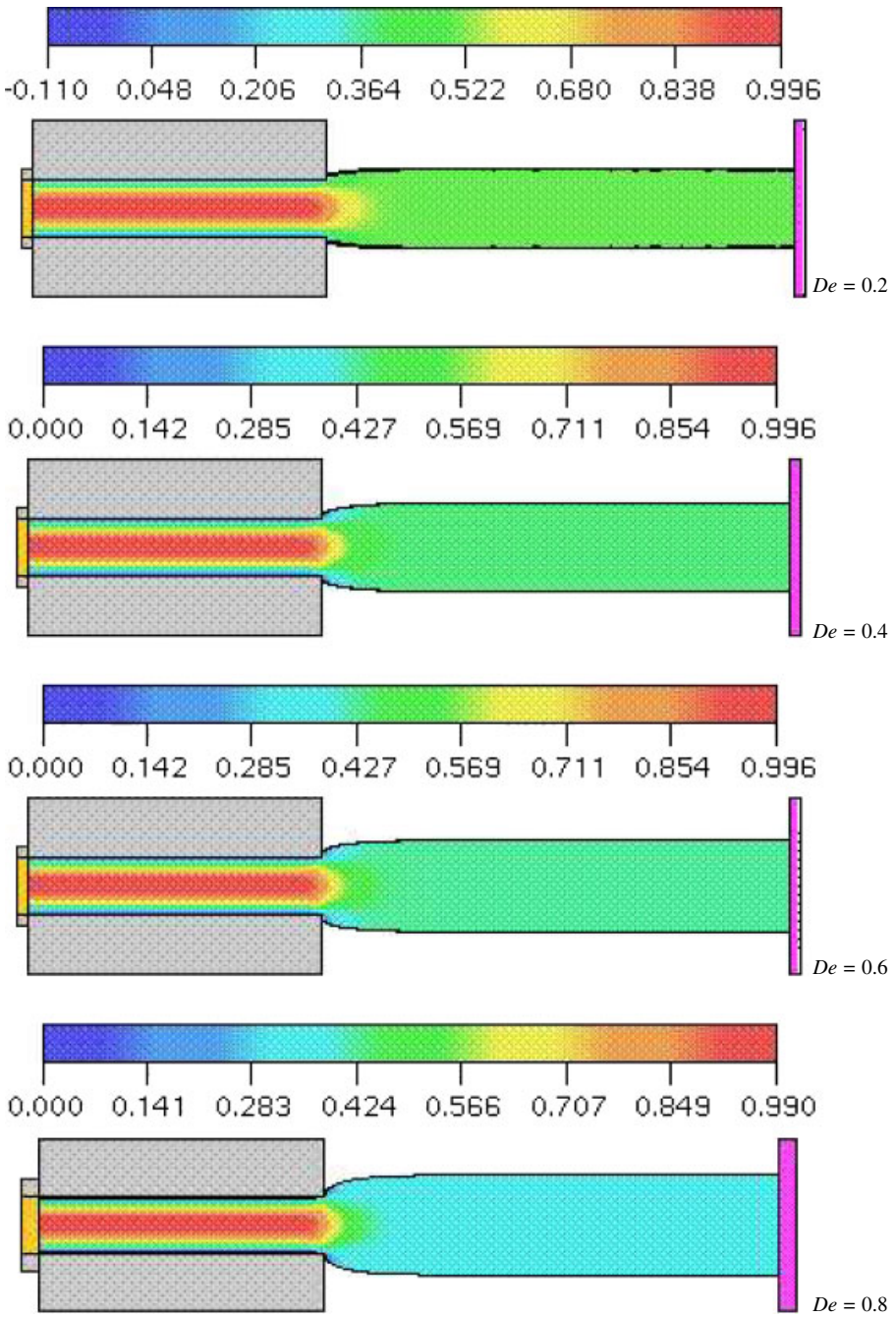

Figure 19. Numerical simulation of the extrudate swell for various Deborah numbers at $t = 0.9$ s. Fluid flow configuration and rendering of the u-velocity.

Copyright © 2006 John Wiley & Sons, Ltd.

DOI: 10.1002/fld

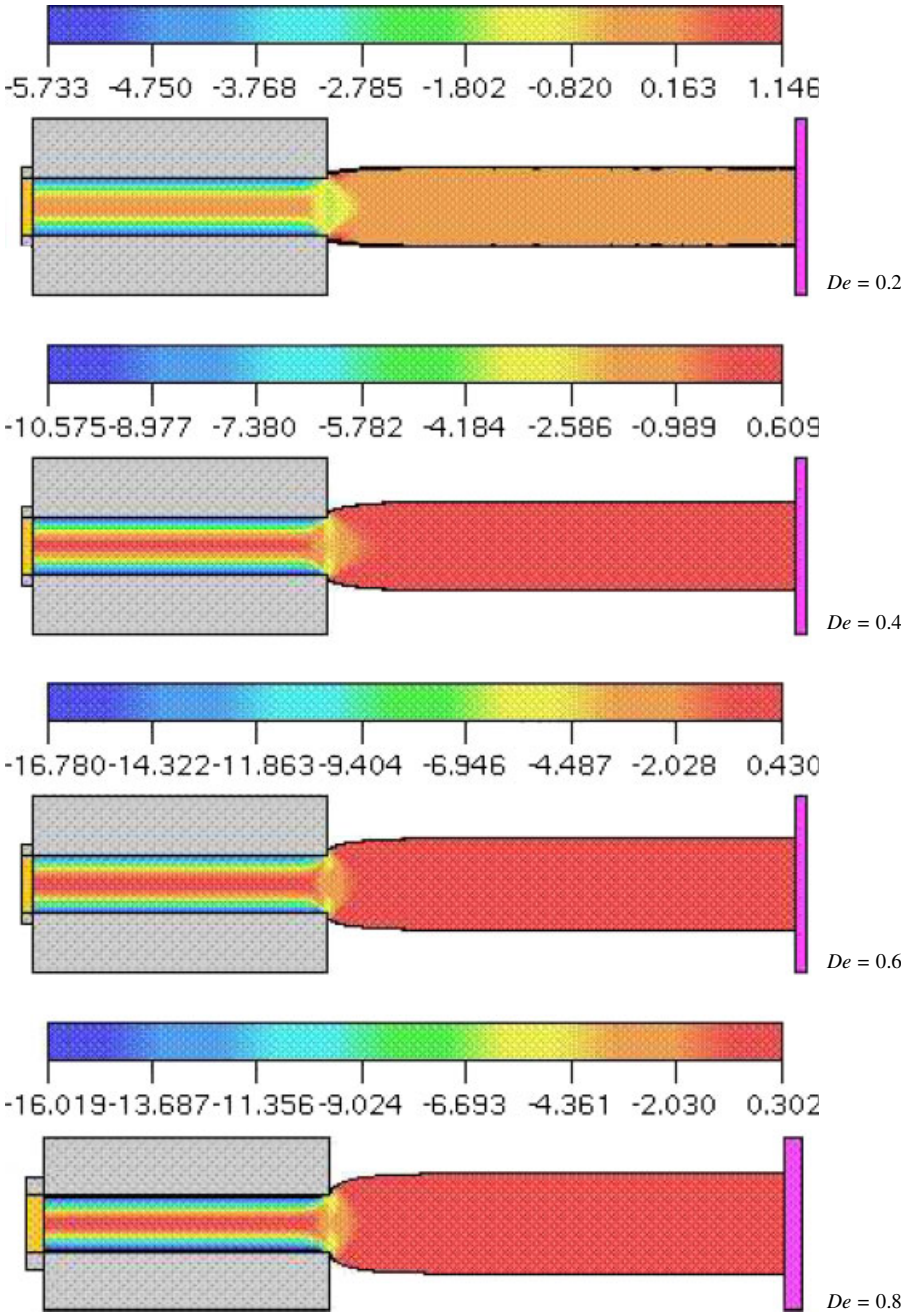

Figure 20. Numerical simulation of the extrudate swell for various Deborah numbers at $t = 0.9$ s. Fluid flow configuration and rendering of the component τ^{xx}.

Copyright © 2006 John Wiley & Sons, Ltd.

DOI: 10.1002/fld

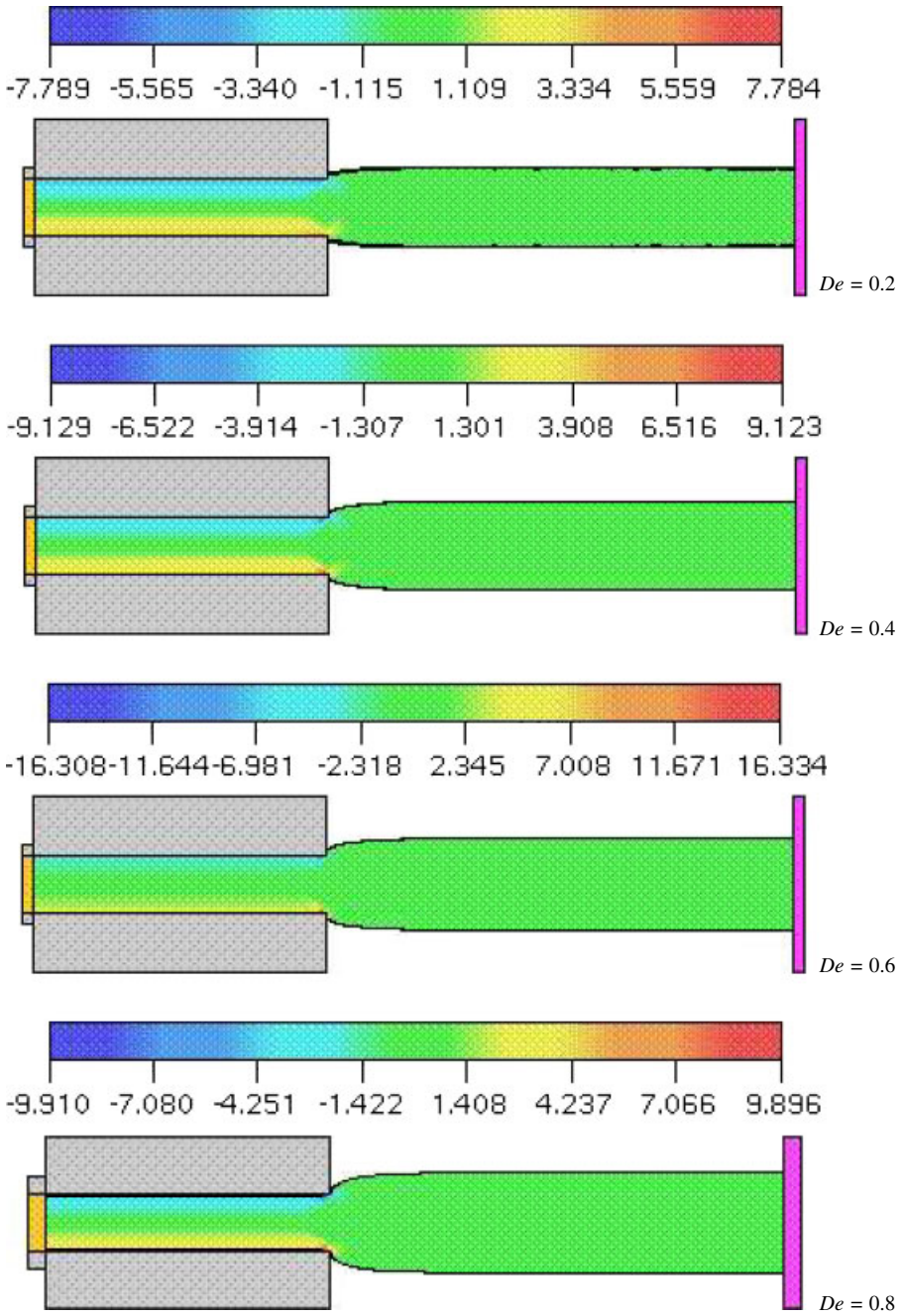

Figure 21. Numerical simulation of the extrudate swell for various Deborah numbers at $t = 0.9\,\mathrm{s}$. Fluid flow configuration and rendering of the component τ^{xy}.

Copyright © 2006 John Wiley & Sons, Ltd.

DOI: 10.1002/fld

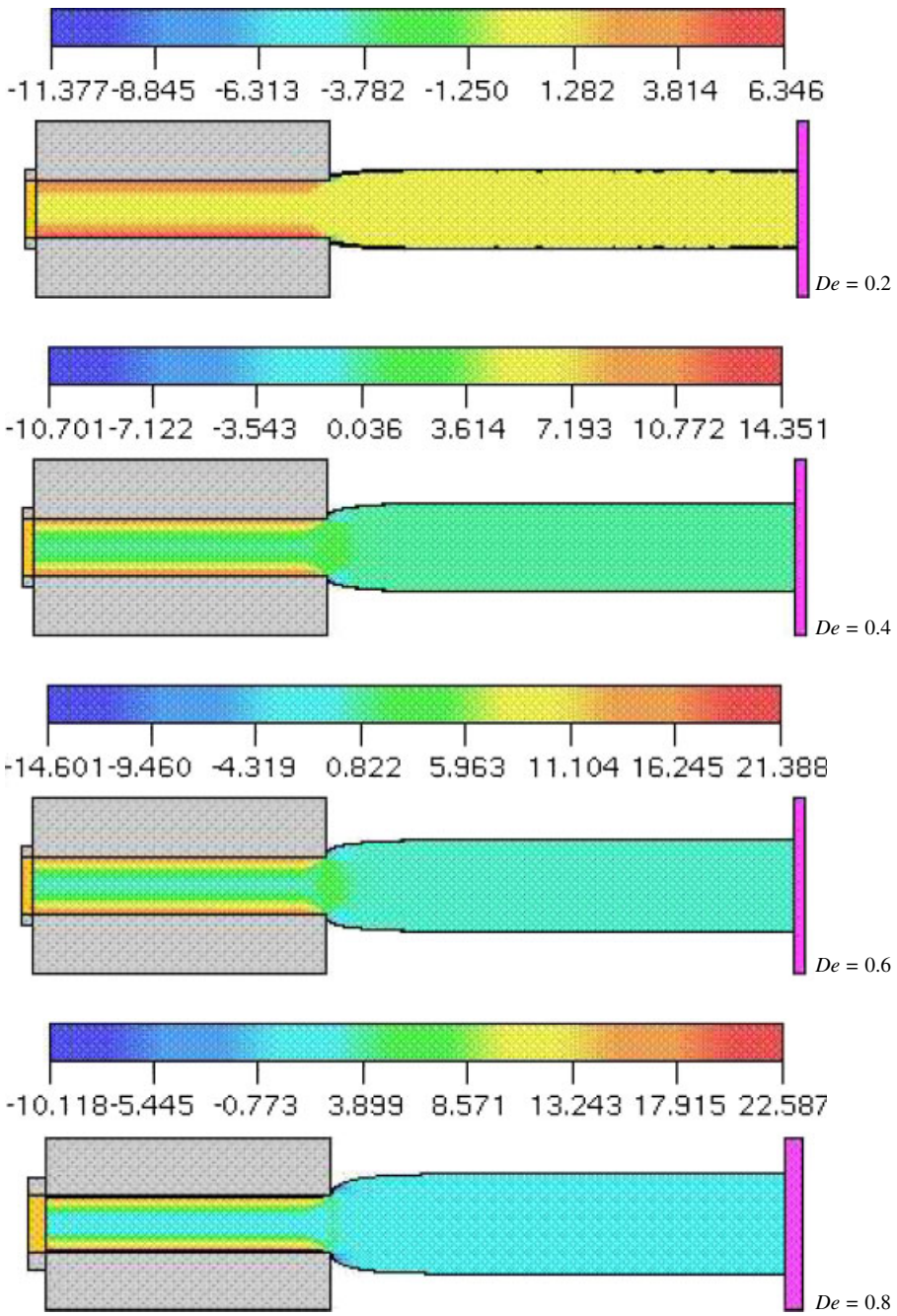

Figure 22. Numerical simulation of the extrudate swell for various Deborah numbers at $t = 0.9$ s. Fluid flow configuration and rendering of the first normal stress difference N_1.

Copyright © 2006 John Wiley & Sons, Ltd.

DOI: 10.1002/fld

$S_r = 1.86$. Thus, we can conclude that the numerical technique developed in this paper can cope with relatively high elastic fluids that are described by the second-order fluid constitutive equation.

7. CONCLUDING REMARKS

This paper presented a numerical technique for simulating two-dimensional free surface flows governed by the second-order fluid constitutive equation. The finite difference equations presented in Section 4 have been implemented into the Freeflow2D [30] code which was then applied to simulate the fully developed flow in a two-dimensional channel. The numerical results were compared with the analytic solution and the agreement was found to be good. Mesh refinement was employed to demonstrate convergence of the numerical technique. Freeflow2D was then applied to simulate the flow through a 4:1 contraction for Reynolds numbers of 0.1 and 1 and various values of the Deborah number. The results showed that as viscoelasticity is increased (as represented by the Deborah number) there is a reduction in the size of the corner vortex. This is in general agreement with the results published in the literature for the 4:1 contraction flow of viscoelastic fluids. Finally, we presented the simulation of the extrudate swell problem for various Deborah numbers. The results demonstrated that the numerical technique presented in this paper can cope with relatively high elasticity described by the second-order fluid constitutive equation.

ACKNOWLEDGEMENTS

The authors would like to acknowledge the financial support of FAPESP (Fundação de Amparo a pesquisa do Estado de São Paulo) (grant no. 00/03385-0) and CAPES (Coordenação de Aperfeiçoamento de Pessoal de Nível Superior) (grant no. 136/05-CAPES/GRICES). The first author has been supported by CNPq (Conselho Nacional de Desenvolvimento Científico e Tecnológico) under grants nos. 474040/2003-8 and 523141/94.

REFERENCES

1. Brasseur E, Fyrillas MM, Georgiou GC, Crochet MJ. The time-dependent extrudate-swell problem of an Oldroyd-B fluid with slip along the wall. *Journal of Rheology* 1998; **42**(3):549–566.
2. Carew EOA, Townsend P, Webster MF. A Taylor-Petrov-Galerkin algorithm for viscoelastic flow. *Journal of Non-Newtonian Fluid Mechanics* 1993; **50**:253–287.
3. Huang X, Phan-Thien N, Tanner RI. Viscoelastic flow between eccentric rotating cylinders: unstructured control volume method. *Journal of Non-Newtonian Fluid Mechanics* 1996; **64**:71–92.
4. Marchal JM, Crochet MJ. A new mixed finite element for calculating viscoelastic flow. *Journal of Non-Newtonian Fluid Mechanics* 1987; **26**:77–114.
5. Phillips TN, Williams AJ. Viscoelastic flow through a planar contraction using a semi-Lagrangian finite volume method. *Journal of Non-Newtonian Fluid Mechanics* 1999; **87**:215–246.
6. Xue S-C, Phan-Thien N, Tanner RI. Three dimensional numerical simulations of viscoelastic flows through planar contractions. *Journal of Non-Newtonian Fluid Mechanics* 1998; **74**:195–245.
7. Yoo JY, Na Y. A numerical study of the planar contraction flow of a viscoelastic fluid using the SIMPLER algorithm. *Journal of Non-Newtonian Fluid Mechanics* 1991; **30**:89–106.
8. Sato T, Richardson SM. Explicit numerical simulation of time-dependent viscoelastic flows problems by a finite element/finite volume method. *Journal of Non-Newtonian Fluid Mechanics* 1994; **51**:249–275.
9. Mompean G, Deville M. Unsteady finite volume of Oldroyd-B fluid through a three-dimensional planar contraction. *Journal of Non-Newtonian Fluid Mechanics* 1997; **72**:253–279.
10. Ryan ME, Dutta A. A finite difference simulation of extrudate swell. *Proceedings of the Second World Congress in Chemical Engineering*, Montreal, vol. VI, 1981; 277–281.

Copyright © 2006 John Wiley & Sons, Ltd.

DOI: 10.1002/fld

11. Crochet MJ, Keunings R. Finite element analysis of die-swell of a highly elastic fluid. *Journal of Non-Newtonian Fluid Mechanics* 1982; **10**:339–356.
12. Tomé MF, Mangiavacchi N, Cuminato JA, Castelo A, McKee S. A finite difference technique for simulating unsteady viscoelastic free surface flows. *Journal of Non-Newtonian Fluid Mechanics* 2002; **106**:61–106.
13. Gast L, Ellingson W. Die swell measurements of second-order fluids: numerical experiments. *International Journal for Numerical Methods in Fluids* 1999; **29**:1–18.
14. *Fidap Manuals*. Fluid Dynamics International. Evanstron: IL, 1995.
15. Harlow F, Welch JE. Numerical Calculation of time-dependent viscous incompressible flow of fluid with a free surface. *Physics of Fluids* 1965; **8**:2182–2189.
16. Bird RB, Armstrong RC, Hassager O. *Dynamics of Polymeric Liquids*, *Fluid Mechanics* (2nd edn), vol. 1. Wiley: New York, 1987.
17. Batchelor GK. *An Introduction to Fluid Dynamics*. Cambridge University Press: Cambridge, MA, 1967.
18. Tomé MF, Duffy B, McKee S. A finite difference technique for simulating Non-Newtonian free surface flows. *Journal of Non-Newtonian Fluid Mechanics* 1996; **62**:9–34.
19. Varonos A, Bergeles G. Development and assessment of a variable-order non-oscillatory scheme for convection term discretization. *International Journal for Numerical Methods in Fluids* 1998; **26**:1–16.
20. Ferreira VG, Tomé MF, Mangiavacchi N, Castelo A, Cuminato JA, Fortuna A, McKee S. High order upwinding and the hydraulic jump. *International Journal for Numerical Methods in Fluids* 2002; **39**:549–583.
21. Tomé MF, McKee S. GENSMAC: a computational marker-and-cell method for free surface flows in general domains. *Journal of Computational Physics* 1994; **110**:171–186.
22. Tanner RI. A theory of die-swell. *Journal of Polymer Science* 1970; **8**:2067–2078.
23. Tanner RI. A theory of die-swell revisited. *Journal of Non-Newtonian Fluid Mechanics* 2005; **129**:85–87.
24. Crochet MJ, Keunings R. Die swell of a Maxwell fluid-numerical prediction. *Journal of Non-Newtonian Fluid Mechanics* 1980; **7**:199–212.
25. Caswell B, Viriyayuthakorn M. Finite element simulation of die swell for a Maxwell fluid. *Journal of Non-Newtonian Fluid Mechanics* 1983; **34**:13–29.
26. Ngamaramvaranggul V, Webster WF. Viscoelastic simulations of stick-slip and die-swell flows. *International Journal for Numerical Methods in Fluids* 2001; **36**:539–595.
27. Clermont JR, Normandin M. Numerical simulation of extrudate swell for Oldroyd-B fluid using the stream-tube analysis and a streamline approximation. *Journal of Non-Newtonian Fluid Mechanics* 1993; **50**:193–215.
28. Cormenzana J, Ledda A, Laso M, Debbaut B. Calculation of free surface flows using CONNFESSITT. *Journal of Rheology* 2001; **45**:237–258.
29. Bush MB. A numerical study of extrudate swell in very dilute polymer solutions represented by the Oldroyd-B model. *Journal of Non-Newtonian Fluid Mechanics* 1990; **34**:15–24.
30. Oliveira J. Desenvolvimento de um sistema de simulação de escoamentos de fluidos com superfícies livres bidimensionais, *M.Sc. Thesis*, ICMC-USP, 1999.
31. McKee S, Tomé MF, Castelo A, Cuminato JA, Ferreira VG. Recent advances in the marker-and-cell method. *Archives of Computational Methods in Engineering* 2004; **11**:107–142.

Copyright © 2006 John Wiley & Sons, Ltd.

DOI: 10.1002/fld